LSPR BASED OPTICAL SENSORS

MAJOR PROJECT PART II REPORT

SUBMITTED IN THE PARTIAL FULFILLMENT OF THE

REQUIRMENTS FOR THE AWARD OF DEGREE

OF

MASTER OF TECHNOLOGY

IN

VLSI DESIGN AND EMBEDDED SYSTEMS

SUBMITTED BY

Ravinder Kaur (2K22/VLS/10)

Under the Supervision of

Dr. Yashna Sharma

(**Assistant Professor**)

Dr. Deepika Sipal

(Assistant Professor)

DEPARTMENT OF ELECTRONICS AND COMMUNICATION ENGINEERING

DELHI TECHNOLOGICAL UNIVERSITY

(Formerly Delhi College of Engineering)

Bawana Road New Delhi, 110042

May 2024

DEPARTMENT OF ELECTRONICS AND COMMUNICATION ENGINEERING

DELHI TECHNOLOGICAL UNIVERSITY

(Formerly Delhi College of Engineering)

Bawana Road New Delhi, 110042

CANDIDATE DECLARATION

I, **Ravinder Kaur Roll No. 2K22/VLS/10** Student of Master of Technology (VLSI design and Embedded Systems), hereby declare that the project Dissertation titled **"LSPR BASED OPTICL SENSOR"** that is submitted by me to the **Department of Electronics and Communication Engineering, Delhi Technological University, Delhi** in the partial fulfilment of the requirement for the award of degree of **Master of Technology** is my original work. I have not plagiarized or submitted the work for award of any other courses. In case if this undertaking is found incorrect, I accept that my degree may be unconditionally withdrawn.

Date: Ravinder Kaur

Place: Delhi 2K22/VLS/10

DEPARTMENT OF ELECTRONICS AND COMMUNICATION ENGINEERING

DELHI TECHNOLOGICAL UNIVERSITY

(Formerly Delhi College of Engineering)

Bawana Road New Delhi, 110042

CERTIFICATE

We hereby certified that the work contained in the Project Dissertation titled "**LSPR BASED OPTICAL SENSORS"** submitted by **Ravinder Kaur Roll No. 2K22/VLS/10** in the partial fulfilment of requirement of awarding Degree **of Master of Technology in VLSI Design and Embedded System to the Electronics and Communication Engineering Department, Delhi Technological University, Delhi** is the record of project work done by student under our supervision. To the best of or knowledge the work has not been presented in part or full other degree of Diploma in this university or anywhere else.

Dr. Yashna Sharma
(Assistant Professor)
ECE Department
DTU, Delhi

Dr. Deepika Sipal
(Assistant Professor)
ECE Department
DTU, Delhi

ABSTRACT

Nano photonics, sometimes referred to as Nano-optics, is the field of research that focuses on the behavior of light at Nano sizes and the interaction between Nano scale objects and light. The interactions are governed by the physical and structural features of nanostructured matter, which take place on a scale that is either the same as or smaller than the wavelength. Nanophotonics has a significant impact on various real-world applications, such as biomedical imaging for diagnosing and treating illnesses, novel imaging systems in cameras, sensors, and sensor systems for chemicals or bioanalytes, as well as nanophotonic devices like switches and modulators for communications. Plasmonics, a subfield of nano photonics, focuses on investigating the resonant interactions that take place at the interfaces between conduction electrons and electromagnetic radiation in metal-dielectric systems.Plasmonics provides the solution. Plasmonics may hold the solution: these technologies can combine the best features of photonics and electronics. Plasmonic devices inherently possess low energy consumption. From a logical and connection perspective, it is possible that this could be the answer. Predictive and preventive maintenance are among the numerous benefits of sensor technology. Not only do they ensure faster delivery of measurement data, but they also enhance accuracy, hence enhancing asset health and process control. Therefore, we will utilize high-efficiency plasmonics to fabricate and simulate a range of sensors and devices.

This article presents a comprehensive examination of the devlopment of plasmonic-besed optical fiber sensors during the last decade. Optical fiber sensing technology is extensively used for the detection and monitoring of chemical, physical, and biological features due to its numerous advantages. In this section, we have provided a concise overview of the historical background, prior experimental investigations on localized surface plasmon resonance (LSPR) [40-41] and propagating SPR. We have finished by discussing potential future directions and discoveries. Advancements in nano-optics have led to the creation of optical systems that do not require labels and are sensitive to changes. This has been achieved by employing SPR and LSPR methods on metal films and nanostructures. This survey focuseing on the significant influence of applications-based fiber optic plasmonic sensors that have been documented in the last decade. This review aims to provide researchers and students with a comprehensive and well-structured summary of the literature on the fundamental principles, latest developments, and practical applications of optical fiber plasmonic sensors.

ACKONWLEGMENT

The success of a project is not just dependent on the work of the assigned individual, but rather relies on the collaboration and oversight of others who have contributed to its completion. I want to extend my admiration to all those who provided support, encouragement, and assistance along my academic journey and in the completion for the project. I would like to extend my heartfelt admiration to my research mentors, **Drs. Yashna Sharma** and **Dr. Deepika Sipal**, for their unwavering encouragement, support, patience, and help throughout this study. I deeply value the recommendations and critiques she offered throughout the project presentation, as they enhanced our skills as presenters. I am delighted to express my gratitude to our families and friends for their invaluable support.

Ravinder Kaur

2K22/VLS/10

TABLE OF CONTENT

LIST OF FIGURES

LIST OF TABLES

LIST OF ABBRIVATION

CMOS……	Complementary metal Oxide Semiconductor
FET ……...	Field Effect Transistor
IC ……..	Integrated Circuits
SPPs……..	Surface Plasmon Polaritons
LSPR……..	Localised Surface Plasmon Resonance
SPR…….	Surface Plasmon Resonance
MF…….	Magnetic Field
TMM…….	Transverse Magnetic Modes
TEM……	Transverse Electric Modes
SERS…….	Surface-Enhanced Raman Spectroscopy
SAM…….	Surface-Active Molecule
VOCs…….	volatile organic compounds
PMCA…….	Poly metha crylic acid
FDTD……..	Finite-Difference Time Domain
FFT……	Fast Fourier Transform
DFT…….....	Discrete Fourier Transform
L…….	Length
PT ……	Plasmonic Technologies
RI……	Refractive Index

CHAPTER 1

INTRODUCTION

Motivation

CMOS technology is consistently reducing in size, in accordance with a pattern that has been apparent over the last five decades. The FinFET transistor was implemented at the latest semiconductor fabrication process, specifically at the 14 nm node. Transistor types such as tunnel FETs, carbon nanotube FETs, and junctionless nanowire transistors are now under investigation to explore the possibility of achieving even smaller nodes [31]. These devices, commonly known as charge-based gadgets, rely on the motion of electrons or holes. Despite the historical trend of increasing scale as depicted in Figure 1.1, is reaching a point of permanent halt due to physical and economic limitations. Nevertheless, the absence of Moore's law does not reduce the need for fast and energy-efficient computing. It is crucial to find alternate solutions to charge-based transistor technology[31].

Plasmonics is a highly promising candidate for replacement. Fig.1.2 depicts the integration of plasmonics, which combine the benefits of photonics and electronics, by leveraging their compact size and fast operation. Photonics is essential for achieving high-speed and large bandwidth Photonics cannot be used in logic circuits because to the diffraction limit of light, despite its high speed. This is the point at which these two technologies separate or differ from each other. This study investigates the utilization of plasmonics in next computing to connect the fields of electronics and photonics. Plasmonics has the potential to surpass the diffraction limit and facilitate the integration of high-speed data processing with small-scale electronics benefits[31].

1.1 Electronics with a speed restriction

The primary factors that limit the speed of ICs are connection delays and heat-relate difficulties. The energy consumption of the IC, which is presently of great significance, is closely linked to heat-related concerns. In a world where computer power is

Constantly increasing but energy consumption is restricted, high-performance applications like server farms must prioritize energy efficiency. This is crucial, given that mobile devices possess a restricted range of batteries and hence necessitate minimal power. Recent advancements have primarily concentrated on achieving same velocity while minimizing energy consumption, or even reducing the velocity to fulfil exceedingly minimal power requirements.

These advancements are primarily targeted towards applications on a big scale. Enlarging the integration of devices, such as the Internet of Things, on a larger scale. Historically, it was customary to augment the Fclk and enhancing performance of the computing components.

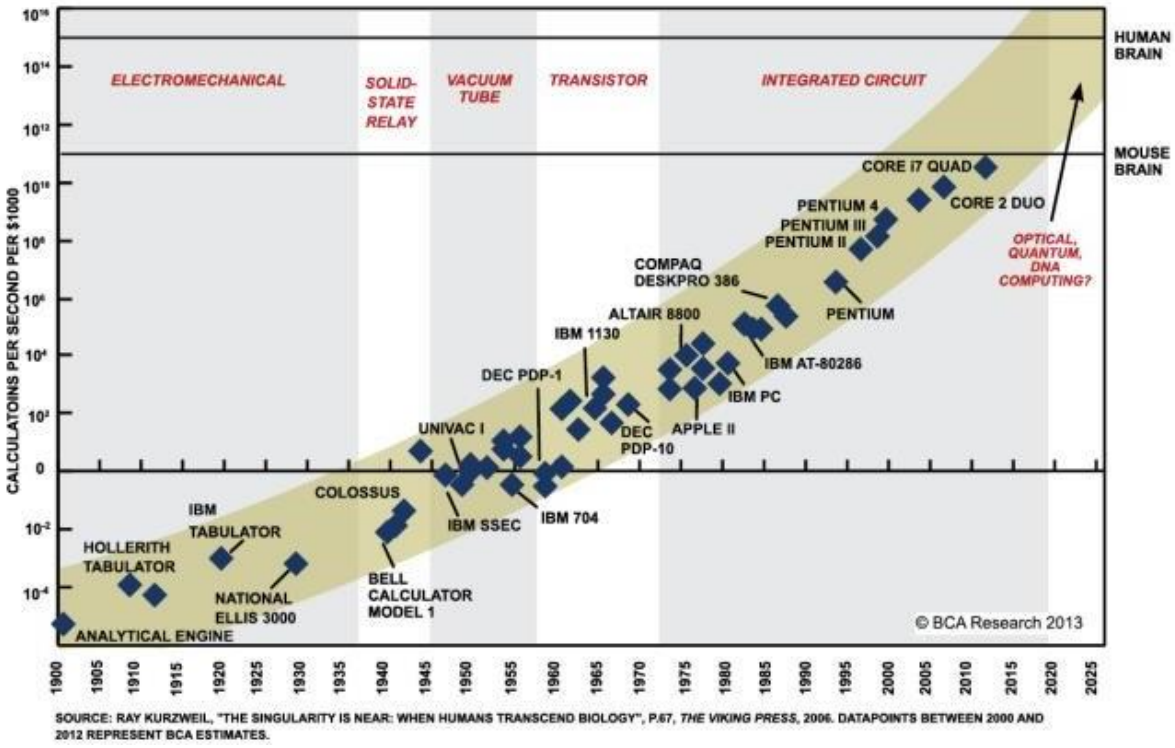

Figure 1.1 Moore's law [39]

1.2 Photonics with diffraction limit

Optical fibers have been employed for extended-range, high-velocity data transmission for a considerable period of time. The development of photonic links has facilitated on-chip communication, leading to the creation of speedier computer applications in recent times. Photonics has a extensive range of frequencies, but ability to decrease in size is limiting by the diffraction limit of light but ability to decrease size is limited by the light wavelength (about 1µm) because of optical diffraction, which hinders the propagation of light at such dimensions.

Photonics is prohibited from being utilized in circuits for dense computing due to this limitation. Photonics surpasses electronics in terms of energy efficiency. However, in order to fully use this benefit, an An efficient stimulation method is necessary. Furthermore, the absence of heat effects in electronics is also a proof

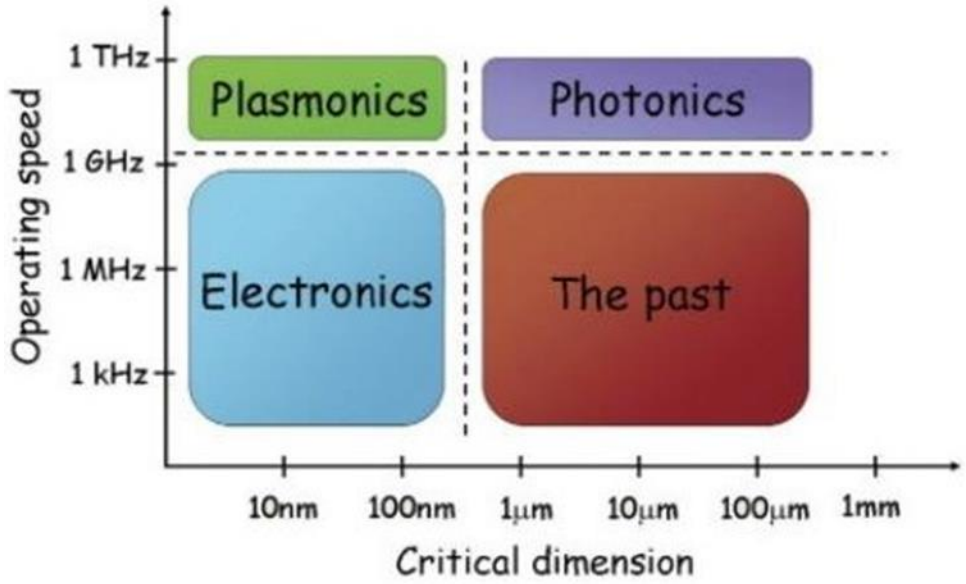

Figure 1. 2. Comparison of electronics, photonics, and plasmonics in terms of speed and size[30]

1.3 Plasmonics as the solution

Fig 1.2 demonstrates PT provide the power to integrate most advantageous characteristics of electronics and photonics. The dispersion relation that characterizes surface plasmon polaritons (SPPs) provides significant evidence for plasmonics[31]. This equation suggests that SPP ICs, in contrast to photonic ICs, can achieve higher density without compromising the speed and bandwidth of light. Furthermore, important to consider incorporation of plasmonic devices in computer applications in the future, along with the development of compact and efficient excitation and detection devices that are currently lacking due to their low energy consumption. Plasmonics could be the solution to achieving both connectivity and logic[30]. An intriguing insight is that plasmonic waveguides can be integrated to serve as both logic devices and

interconnects. This dissertation does not try to provide evidence that plasmonic technology is the optimal answer, yet it is a significant assertion.

Both photonics and electronics, which are extensively utilized, are poised to revolutionize computer and data transmission applications in the foreseeable future. Lately, there has been a significant amount of emphasis focused on LSPR, which has been extensively researched at the nanoscale. These resonances result in prominent scattering peaks and significant increases of the electromagnetic near-field when linked to noble metal nanostructures. The synthesis of noble metal nanostructures has advanced significantly over the past 10 years, which has aided in the expansion of LSPR research and technology across a number of fields. Using alterations in the LSPR spectral peak to pinpoint chemical interactions near the nanoparticle surface is one method among them[31]. We present a high-level overview of this sensing methodology here. We are unable to assert that our Review is comprehensive because this is a topic that is always growing. However, we will attempt to list the primary research projects in this area and should go over a wide variety of relevant literature. Nanoparticles of gold or silver have been utilized in the most of the research on LSPR sensing. Because of its chemically stability and restriction to oxidation, gold is usually used, however silver has stronger resonances and a better sensitive to the refractive index. By contrasting Au and Ag nanoparticles with comparable size or shapes, this is illustrated [31].

CHAPTER 2

Study on plasmons and SPPs

A comprehensive comprehension of surface plasmon physics is necessary for the construction of plasmonic devices. SPPs can be classified into two categories: localized and propagating. Given that plasmons serve as conveyors of information, this study will primarily concentrate on the propagation of SPPs[31] . Initially, a description of plasmons and (SPPs) is provided to offer the reader a basic grasp of plasmonics. The dispersion relation that characterizes the SPPs for a single contact will be determined once certain fundamental elements from the field of electromagnetics are obtained and examined. The focal point of the discussion will be the compromise between confinement and transmission length in plasmonic waveguides [31].

.

2.1 An Instinctual approach to plasmonics

The Valence electrons in a metal can be conceptualized like an electron plasma or a gas composed of freely moving electrons [31]. Electrons exhibit oscillatory motion when subjecting to an outer field. A plasmon refers to a discrete unit of oscillation in the charge of a quantum. The term "volume plasmon" is used to specifically represent the actions of plasmons in bulk materials. The focus of this work is on the exploration and application of SPPs, which are a type of plasmons [31]. A SPP is a wave that propagates by connecting the oscillations of electron plasma to electromagnetic fields. To view a basic diagram of Surface Plasmon Polaritons (SPPs), refer to Figure 2.1(a). SPPs occur exclusively at the boundary between a dilectric material, through which the EM field propagates, and a conducter that sustains oscillation of electron plasmas. The E field amplitude of the SPP wave rapidly decreases in the opposite direction to its propagation[31]. .Figure 2.1(b) demonstrates that the field diminishes rapidly when entering the metal and at a slower rate when entering the dielectric. Containment and guiding are essential attributes for

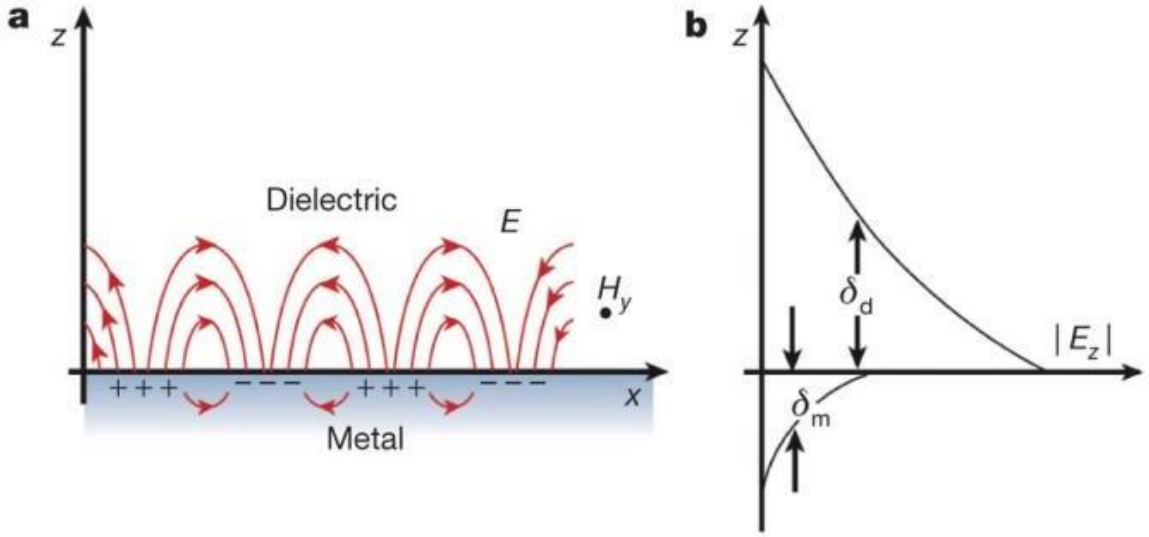

Figure 2.1. show the following: a) a SPP schematic; b) the E- field Ez's exponential decay with respect to the direction of propagation. The decay L into the M-∈ are indicated by δm and δd, respectively[31].

2.2 Electromagnetics

2.2.1 Dielectric function of free gas electron

The dielectric function of a substance represent its response to an external EM field. For the purpose of to ascertain the dielectric function of the free electron gas, a fraction of a conductor is exposed to an external electric field, as seen in Fig 2.2. This field will induce the electrons to displace from the (+ve) ions. However, the electron's velocity will decrease due to Collisions [31]. This phenomenon is understood by considering the τ of the electron gas, which is compared to the freq of collisions.

$$\gamma = 1 / \tau$$

The free electron gas's equation of motion is provided by:

$$m_e \ddot{x} + m_e \gamma \dot{x} = -eE, \qquad (2.1)$$

where E is the applied E field, e is the elementary charge, and m_e is electron mass. Assume that E(t) = $E_0 e^{-i\omega t}$ is the harmonic time dependency of the external field. The following expression represents the movement of the free electron gas: P = $-n_e ex$ [31]

$$x(t) = \frac{e}{m_e (w_2 + ijw)} E(t) \tag{2.2}$$

The displacement at a specific point in time is shown in Figure 4 as 4x. When the displcement expression (Eq. (2.2) is substituted, the P = $-n_e ex$ is as follows:

$$P = \frac{-n_e\ e^2}{m_e (w_2 + ijw)} E(t) \tag{2.3}$$

Where n_e is the metal's electron density. Applying the relation for the following yields the dielectric function electric displacement field[31] D = $\in_0$E + P:

$$D = \in_0 (1 - \frac{n_e\ e^2}{\in_0 m_e (w_2 + ijw)})E \tag{2.4}$$

The plasma frequency ω_p can be defined as:

$$\omega_p = \frac{-n_e\ e^2}{\in_0 m_e} \tag{2.5}$$

$$D = \in_0 (1 - \frac{\omega_p^2}{(w_2 + ijw)})E \tag{2.6}$$

Moreover, the permittivity ∈(ω) may be derived since D = ∈0∈(ω) E: [31]

$$\in(\omega) = (1 - \frac{\omega_p^2}{(w_2 + ijw)}) \tag{2.7}$$

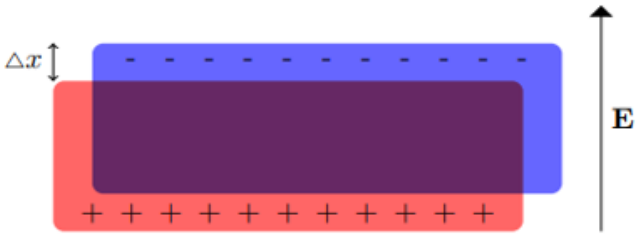

Figure 2.2. Electron Plasm Displacement [31]

2.2.2 Drude Model

To get the Re and Im components of a metal's relative permittivity, reorganize equation (2.6) as follows: $\in(\omega) = \in R + i \in I$

$$\in(\omega)= \left(1 - \frac{\omega_p^2}{\omega^2+\gamma^2}\right) + i\left(\frac{\gamma\omega_p^2}{\omega^3+\omega\gamma^2}\right) \quad (2.8)$$

This can be reduced to when the frequency ($\omega >> \gamma$) is much higher than the collision frequency.

$$\in(\omega)= \left(1 - \frac{\omega_p^2}{\omega^2}\right) + i\left(\frac{\gamma\omega_p^2}{\omega_p^3}\right) \quad (2.9)$$

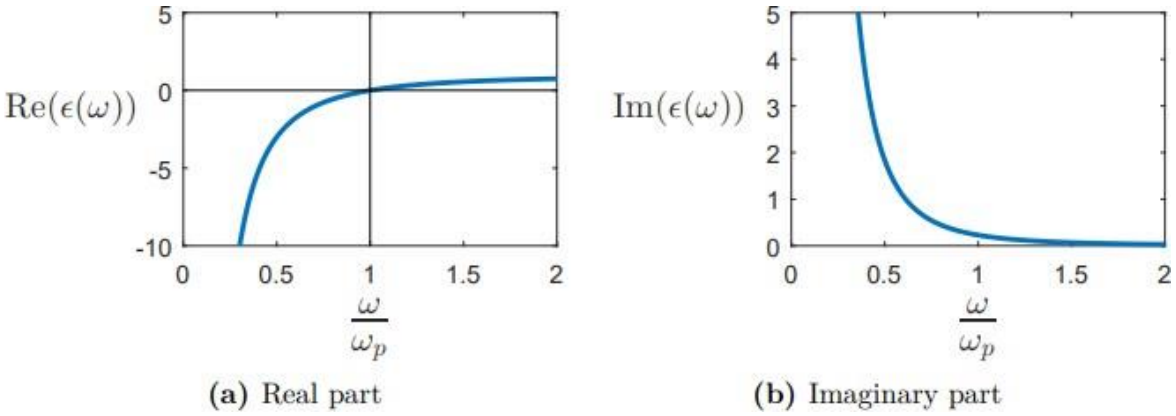

Figure 2.3. Drude model-derived permittivity

Figures 2.3(a) and 2.3(b) depict the graphed Re and Im parts of the (2.9). The real part arises due to a delay in the phase between the ele. and mag. fields, whereas the Im part is associated with the absoption of energy in material being investigated [31]. Obtained permittivity here will be necessary for the subsequent calculations of grop velocity and dispersion relation for the SP Ps.

2.2.3 Wave Equation

SPPs arise from the coupling bet the oscillation of the electron plasma and EM fields. EM wave equation is necessary to explain the transmission of SPPs. Hence, the subsequent section deduces this equation, and to commence, we necessitate Maxwell's equations [31]:

$$\nabla . D = \rho \quad (2.10\ a)$$

$$\nabla . B = 0 \quad (2.10\ b)$$

$$\nabla X E = -\frac{\partial B}{\partial t} \quad (2.10\ c)$$

$$\nabla X H = J + \frac{\partial D}{\partial t} \quad (2.10\ d)$$

Utilizing B = μ_0(H + M), assuming M = 0 magnetization, extract the curl from (2.10c) to obtain:

$$\nabla \text{ X } \nabla X E = \nabla X \left(-\mu_0 \frac{\partial H}{\partial t}\right) = -\mu_0 \frac{\partial(\nabla X H)}{\partial t} \quad (2.11)$$

When equation (2.10d) is inserted, this becomes:

$$\nabla \text{ X } \nabla X E = -\mu_0 \frac{\partial J}{\partial t} - \mu_0 \frac{\partial^2 D}{\partial t} \quad (2.12$$

For the rest of this work, we make the assumption that there are no current densities or external charges. Subsequently, the previous assertion can be reformulated in the following manner[31]:

$$\nabla^2 E - \frac{\epsilon}{c^2}\frac{\partial^2 E}{\partial t} = 0 \quad (2.13)$$

$$\nabla^2 E + k^2 \epsilon E = 0 \quad (2.14)$$

2.3 SPPs at an interfaces

Utilizing outcomes of preceding section, specifically the Helmholtz equation (2.14), it is now possible to deduce equations for surface plasmon polaritons[31]. There are certain restrictions placed on the way the propagation geometry works, as depicted in Figure 2.4: To ensure clarity in the subsequent derivations, we will consider a planor waveguide with a Cartesien coordenate

system. The permittivity is solely determined by the z-coordinate when waves propagate in x-direction, but the electric field remains constant in the y-direction: $\Delta = \in(z)$. Furthermore, the surface at z = 0 is the medium through which surface plasmon polaritons propagate. The waves propagating on the interface can be represented by the equation E(x, y, z) = E(z) e^iβX, given certain simplifications. The parameter β, which is equal to the product of k and x, represents the complex. The substitution of the above expression for E in equation (2.14) results in the wave equation.

$$\frac{\partial^2 \mathrm{E}}{\partial \mathrm{z}} + (\mathrm{k}_0^2 \, \epsilon - \beta^2) \, \mathrm{E} = 0 \qquad (2.15)$$

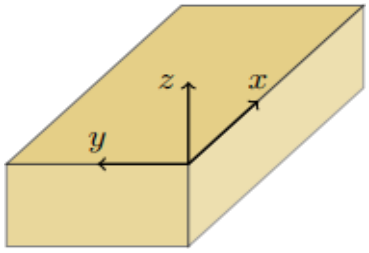

Figure 2.4. Geometry of propagation

To calculate the disparsion relation and spatial field profiles of propagting surface plasmon polariton (SPP) waves, it necessery to obtain the field components of the electric (E) and magnetic (B) fields [31]. The equation is for Maxwell's curl, namely equetions (2.10 c) and (2.10 d), can be utilized to calculate them. Again, it is presumed that M$\boldsymbol{\partial x}$ equals zero and that the time dependence of the harmonics is given by $\boldsymbol{\partial y}$=−iω. The extent of the curl of a vector field is as follows.

$$\nabla X \, F = \left(\frac{\partial F_3}{\partial y} - \frac{\partial F_2}{\partial z}, \frac{\partial F_1}{\partial z} - \frac{\partial F_3}{\partial x}, \frac{\partial F_2}{\partial x} - \frac{\partial F_1}{\partial y} \right) \qquad (2.16)$$

Following the same order as in equation (2.16), the first curl equation (2.10c)'s elaborated components is [31]:

$$\frac{\partial E_Z}{\partial y} - \frac{\partial E_y}{\partial z} = i\omega\mu_0 H_x \quad (2.17a)$$

$$\frac{\partial E_x}{\partial y} - \frac{\partial E_z}{\partial z} = i\omega\mu_0 H_y \quad (2.17b)$$

$$\frac{\partial E_y}{\partial y} - \frac{\partial E_x}{\partial z} = i\omega\mu_0 H_z \quad (2.17c)$$

Using the identical procedare to the second curl equation (2.10d), the subsequent outcomes are acquired:

$$-\frac{\partial E_y}{\partial z} = i\omega\mu_0 H_x \quad (2.19a)$$

$$\frac{\partial E_x}{\partial z} - \mathrm{i}\beta E_z = i\omega\mu_0 H_y \quad (2.19b)$$

$$\mathrm{i}\beta E_y = i\omega\mu_0 H_z \quad (2.19c)$$

$$\frac{\partial H_y}{\partial z} = = i\omega\epsilon\epsilon_0 E_x \quad (2.20a)$$

$$\frac{\partial H_x}{\partial z} - \mathrm{i}\beta H_z = - i\omega\epsilon\epsilon_0 E_y \quad (2.20b)$$

$$\mathrm{i}\beta H_y = i\omega\epsilon\epsilon_0 E_z \quad (2.20c)$$

These set of equations allows for two different solutions for the propagating waves, each with a different polarization. These solutions are known as the TM and TE modes [24]. The only field componants that are not = 0 in TM modes (transverse magnetic modes) are Ex, Ez, and Hy. The only field component that are not = 0in TE modes (transverse electric modes) are Ht, Hz, and Ey. Figure 2.5 demonstrates

.

Figure 2.5. Waveguide modes

TM modes are derived by selecting just the non-zero elements from equations (2.20a) and (2.20c).

$$E_x = -\frac{i}{\omega\epsilon\epsilon_0}\frac{\partial H_y}{\partial z} \tag{2.21a}$$

$$E_z = -\frac{\beta}{\omega\epsilon\epsilon_0}H_y \tag{2.21b}$$

If two of the equations in (2.19b) are completed, the wave equation for TM mode is:

$$\frac{\partial^2 H_y}{\partial \mathrm{z}} + (\mathrm{k}_0^2\,\epsilon - \beta^2)H_y = 0 \tag{2.21c}$$

For TE modes, the same procedure can be used, and the result is:

$$H_x = \frac{i}{\omega\mu_0}\frac{\partial E_y}{\partial z} \tag{2.22a}$$

$$H_z = \frac{\beta}{\omega\mu_0}E_y \tag{2.22b}$$

Along with the associated wave equation

$$\frac{\partial^2 E_y}{\partial \mathrm{z}} + (\mathrm{k}_0^2\,\epsilon - \beta^2)E_y = 0 \tag{2.22c}$$

These formulas enable us to compute the solutions for SPP wave propagation at various types of interfaces [31]. Figure 2.7 displays the mode field, whereas Fig 2.8 illustrates the dispersion relation.

2.3.1 SPPs at Single interface

The bunches of equations (2.21) and (2.22) can be utilized for analysing a metal-dielectric interaction. Figure 2.6 provides a basic representation that allows one to gain general understanding of the propagation of SPPs [31]. The figure depicts the relative permittivity, or dielectric constant, of M and $\in$ as εd and εm, respectively. Due to the constraints imposed by equations (2.22), solutions for SPP waves are not applicable for TE modes. Therefore, only the for TM modes solution are taken into consideration in this context. It is important to mention that in practicl applications, less optimal propagtion geometries are employed instead of the two semi-infinite sections that have been examined up to this point. As a result, both TM and TE modes will

make up the propagating modes. Nevertheless, similar to mixed modes, the answers in TM-mode and the subsequent discussion offer an equivalent qualitative comprehension.

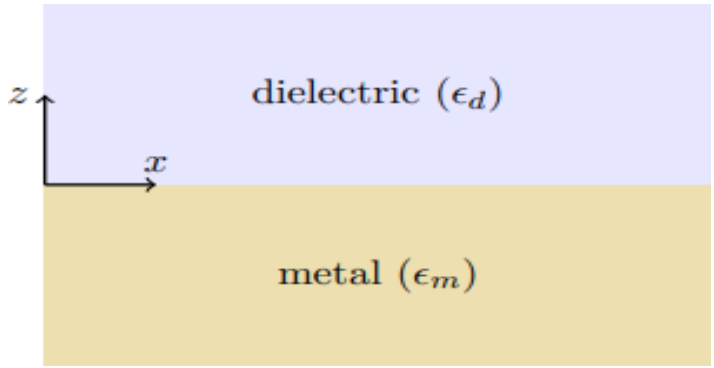

Figure 2.6 Single M-∈ interface

Equation (2.21) can be applied for get the E field components for the dielectric area (z > 0) with the two semi-infinite sections [31]:

$$E_x\,(z) = C_1 \frac{i}{\epsilon_0 \epsilon_d \omega} k_{z,d} e^{-k_{z,d} z} e^{i\beta x} \tag{2.23a}$$

$$E_z\,(z) = -\,C_2 \frac{\beta}{\epsilon_0 \epsilon_d \omega} k_{z,d} e^{-k_{z,d} z} e^{i\beta x} \tag{2.23b}$$

$$H_y = C_1 e^{-k_{z,d} z} e^{i\beta x} \tag{2.23c}$$

metal component (z < 0):

$$E_x\,(z) = -\,C_2 \frac{i}{\epsilon_0 \epsilon_d \omega} k_{z,m} e^{-k_{z,m} z} e^{i\beta x} \tag{2.23d}$$

$$E_z\,(z) = -\,C_2 \frac{\beta}{\epsilon_0 \epsilon_m \omega} k_{z,d} e^{-k_{z,m} z} e^{i\beta x} \tag{2.23e}$$

$$H_y = C_2 e^{-k_{z,m} z} e^{i\beta x} \tag{2.23f}$$

The relation in ele and mag. Implies that the wave vectors kz,d and kzm represent the wave vectors that are | to the direction of propagation and are directed into the M and ∈, resp. The constants C1 and C2 are present in these fields. The Dz-field at a air-Au contact and at λ of 1550 nm can be graphed using equations (2.23b) and (2.23e) [31]. Figure 2.7 depicts this phenomenon for both the metallic region where (z < 0) and the dielectric region where (z > 0). The y-axis

ranges of the two graphs differ by a factor of 50, suggesting that the electric field diminishes within the metal significantly faster than within the dielectric.

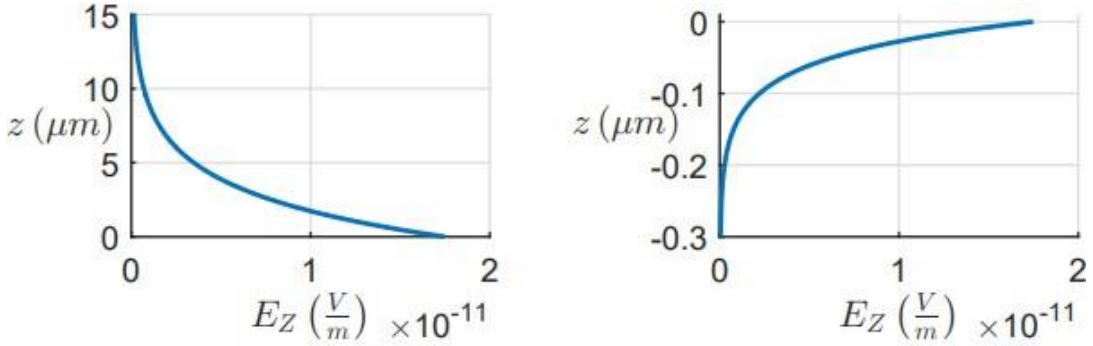

(a) E_z-field in the dielectric **(b)** E_z-field in the metal

Fig 2.7. Decrement of the E_z field [31]

Since equations (2.23) and (2.24) in both sections are continuous at z = 0, C1 = C2 and.

$$\frac{\epsilon_d}{\epsilon_m} = -\frac{k_{z,d}}{k_{z,m}} \tag{2.25}$$

The relation (2.25), assuming positive integers for $k_{z,d}$, kzm, and ϵ_d, implies that Re [ϵ_m] is less than 0. This suggests that the 2nd material, assuming a chosen dielectric, must a metal with a (-ve) Re [permittivity] down the ω_p [31]. The expression for the M field H_(y) is derived based on the equation of wave for TM modes (2.21c) and the boundary conditons at z = 0. When (2.23c) ad (2.24c) are substituted in equation (2.21c), the wave vectors for the metal and dielectric are given as (2.26a) and (2.26b) respectively

$$k_{z,d}^2 = \beta^2 - k_0^2 \in_d \tag{2.26a}$$

$$k_{z,m}^2 = \beta^2 - k_0^2 \in_m \tag{2.26b}$$

Finally, equations (2.26) and (2.25) can be utilized to derive the dispersive relation of propagating SPPs at a M-dielectric interface [31].

$$\beta = \frac{\omega}{c}\sqrt{\frac{\epsilon_d \epsilon_m}{\epsilon_d + \epsilon_m}} \tag{2.27}$$

An alternative approach to expressing the dispersion relation involves utilizing the (ϵ(d)=1) and a considering the usage of a metal without any absoption losses (as determined by the real component from Equation (2.9)).

$$\beta = \frac{\omega}{c}\sqrt{\frac{\omega^2 - \omega_p^2}{2\omega^2 - \omega_p^2}} \tag{2.28}$$

By mapping out this correlation, it becomes possible to analyze and discuss the different locations. This analysis is specifically conducted for a surface plasmon polariton (SPP) confined to a single contact between air and Au, as depicted in Fig 2.6 [31]. The dispersive relation is determined in Figure 2.8.

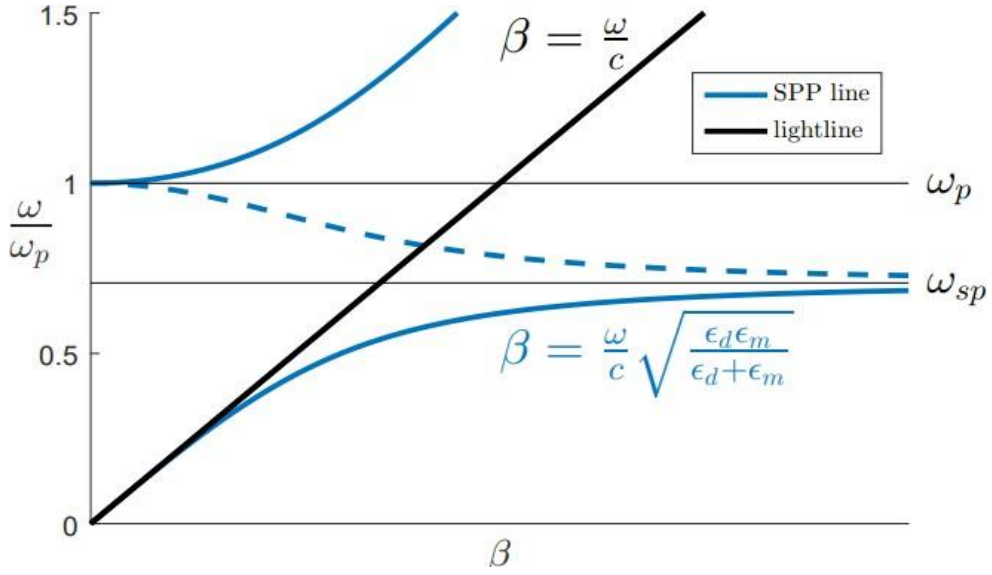

Figure 2.8. Plotting the Re component (continue line) and Im part (dash line) of an SPP at single interface between semi-infinite Au and air sections shows the dispersion relation [31].

The dispersion relation, often known as the light line, for a free photon is represented as a reference point. β = kx is a complex number, consisting of a real factors represented by a stronge line and an imaginary component represented by a doted line[31]. Due to the small magnitude of the k-vector c and the alignment of the SPP curve with the light line at low frequencies, the wavelengths are higher [31]. At highest frequncies, SPP curve exhibits a downward curvature, while the k-vector β increases in magnitude compared to the light line. This indicates that the wavelengths at that frequency are smaller. The surface plasmon frequency, wsp, represents the point at which the curve approaches an asymptote[31]. When the frequency reaches this value, vg = ∂ω/∂k, = 0 which

means that the surface plasmon mode remains stationary. The frequency measurement is supplied by

$$\omega_{sp} = \frac{\omega_p}{\sqrt{1 + \epsilon_d}} \tag{2.29}$$

The dashed line indicates that there is no transmission of Surface Plasmon Polaritons (SPPs) between wsp and wp due to the purely hypothetical nature of the propagation constant. Electromagnetic waves are emitted into metal greater then wp due to the initiation of oscillation in the bulk electron plasma. In this section, the relations of field for TM modes at a M-ϵ interface was derived and may be found in equations (2.23) and (2.24)[31]. By employing these equations, we can calculate the group velocity and confinment of a SPP at the interface between M-ϵ a by establishing the dispersion relation (2.27).

CHAPTER 3
PLASMONIC SENSING

Both SPR and LSPR are extensively used in various sensing applications, including humidity sensors, refractive index sensors, and DNA sensors. This is due to their ability to enhance the electric field at the surface, with SPR occurring at the planar interface and LSPR occurring at the surface of nanoparticles. However, the choice between SPR and LSPR based sensing is critical, depending on whether bulk or localized sensing is needed. The reason for this is that, as seen in Fig. 11(a)–(b), both SPR and LSPR exhibit different decay lengths as one moves further from the surface. The evanescent plasmon field in LSPR decays rapidly, with a decay length of approximately 20-40 nm. In contrast, the decay of the SPR evanescent field is slower, with decay lengths ranging from 100-200 nm depending on the specific metal and dielectric. Due to the fact that molecular binding events, such as antigen-antibody binding or DNA detection, take place very close to the surface at scales of just a few nanometers, LSPR-based sensors are better suited for sensing applications that involve these types of events. Figure 3.1 (c) depicts an LSPR-based sensor that is affected by the captured analysts, resulting in localized changes near the surface and subsequently modifying the LSPR wavelength. Unlike LSPR, SPR-based sensors are suitable for detecting changes in the RI of the bulk medium. This is due to their long decay lifetimes, which give them a higher sensitivity to bulk change. The SPR sensors are not effective in detecting changes that occur on a small scale closer to the surface

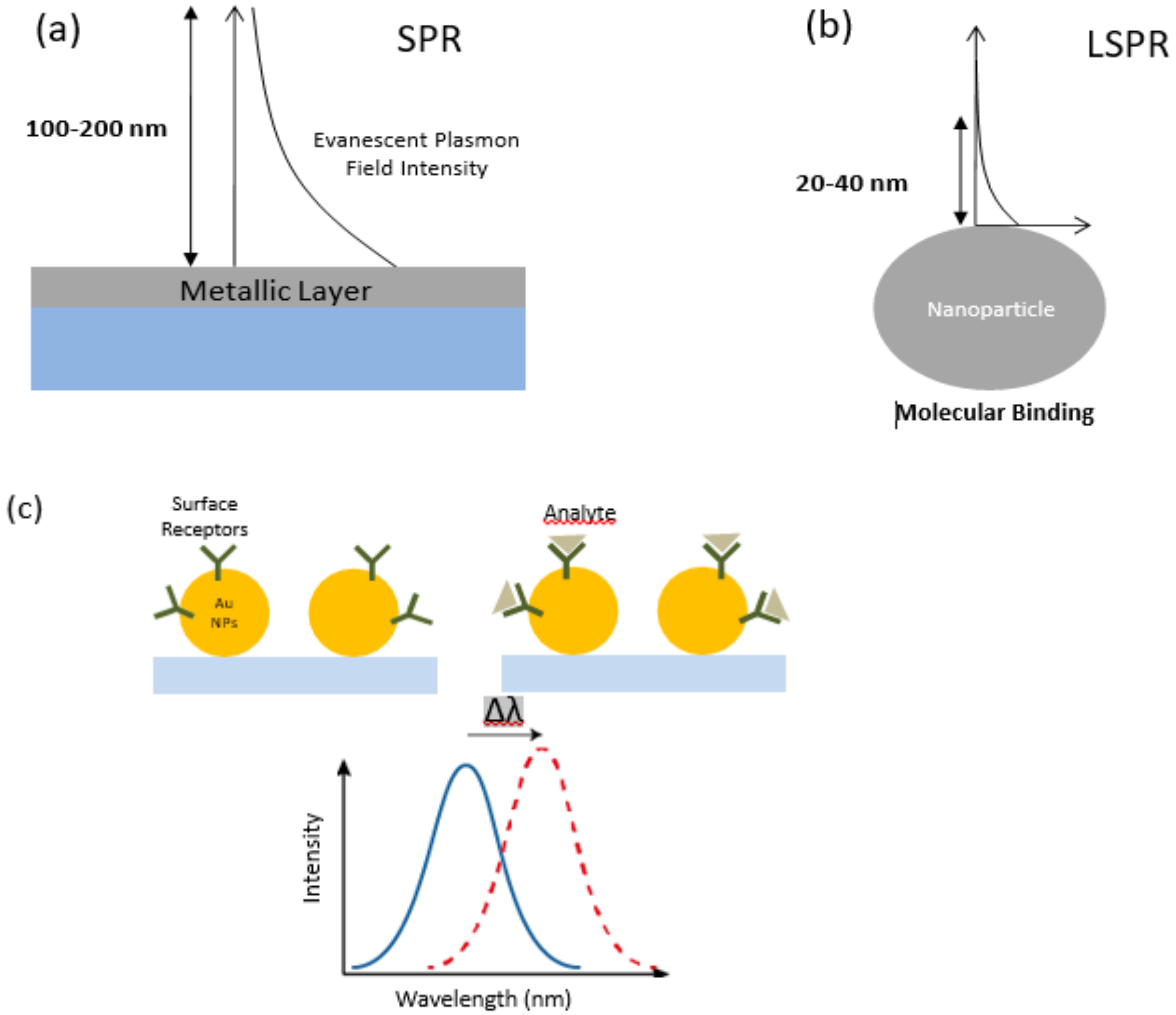

Figure 3.1. The figure showing (a) bulk sensing using SPR (decay lengths ~100-200 nm allow efficient SPR sensing), and (b) localized sensing using LSPR (decay lengths ~20-40nm allow for localized sensing). (c) Surface receptors are attached to plasmonic nanoparticles to sense analysts. On attachment of the analysts to the surface receptors, the LSPR peak shifts from one wavelength to another, which can be efficiently recorded

The identification of analytes, including chemical and biological agents, is increasingly important in the current day. These applications encompass the identification of various chemical compounds, including pesticides, pharmaceuticals, combustion by-products, explosives, and chemical warfare agents. Additionally, they involve the detection of bio-agents such as cancer genes and anthrax markers. In most cases when highly specific sensing is necessary, the analyte of interest is usually found in a mixture of other chemicals or water, which needs to be removed before detection. Therefore, it is necessary to have a sensing technology with a sufficiently high

resolution in order to distinguish individual chemicals in a background or while dealing with a mixture of identical analytes. Previous advancements in the field have led to the development of techniques such as immuno-absorbent assays and ELISA. However, these techniques are limited in their ability to provide precise spatial resolution and sensitivity. Several spectroscopy techniques have lately been studied to identify chemical and biological substances. Due to its distinct advantages compared to other methods, plasmonics-based sensing has emerged as one of the most efficient spectroscopic techniques currently accessible. For example, SERS can be utilized to identify analytes even at concentrations as low as sub-picomolar or when it is essential to detect individual molecules.

3.1 Physics of LSPR

Plasmons are formed when free electrons of a noble metal collectively oscillate. The -on suffix is derived from its characterization as a unit of plasma oscillation in quantum physics [5]. However, it should be noted that this terminology can be somewhat deceptive, as the phenomenon can be adequately explained using conventional physics. When a metal is subjected to an outer electric field, the electron gas within the metal undergoes mechanical oscillations, cause of electrons to move in resp to the stationary ionic cores [7] The occurrence is referred to as plasmon oscillations. Bulk plasmons exhibit oscillations with energy that occur at the plasma frequency.

$$\boldsymbol{E_p = \hbar\sqrt{\frac{ne^2}{m\epsilon_0}}} \qquad \textbf{(3.1)}$$

Where n is the electron density, e is the charge of electron, m is the mass of electron, and ε0 is the permittivity of free space. Surface plasmon polaritons, or simply surface plasmons, are the form that plasmons take at the surface of a metal. Through a grating or a flaw on the M -surface, light can be linked into standeng or propageting SP modes. Surface plasmons are optically stimulated. Light that couples most effectively has a high incedence angle or with wave vector k almost parallel to the surface. This is because SPs excited by the circular E- field of the forwarding plane wave[11]. A SP that limited towards nanoparticle—a particle with a size same to the λ—is known as a LSP because free electrons take part in the colletive oscillations. The LSP has two significant outcomes. First, there is a significant augmentation of electric fields in the vicinity of the surface of the partical ; this increment is highest on a surface and decreases w.r.t distance. 2nd, for noble

metal nanoparticles, the optical extinction of the particle reaches its maximum at the PR frequency, which happens at visible wavelengths [15]. This extinguishment peak, which is the foundation for the sensing applications covered in this Review, is dependent upon the surrounding medium's refractive index. We must use scattering theory to fully comprehend how this LSPR forms

3.2 Mie's Theory

Gustav Mie [41] gave an analyse based solution to Maxwell's equations, which elucidate the function of light scattering and absorption by spherical particles, during the early 20th century [40-41]. The widely recognized phenomenon of Rayleigh scattering is equivalent to Mie scattering for particles of extremely small size.

The variables used in the expression are d and λ. The total scattring, extinction, and absorption cross-sections can be determined by identifying the dispersed fields resulting from the interaction of a plane wave with a same conducting sphere.

$$\sigma_{ext} = \frac{18\pi\epsilon_m^{\frac{3}{2}}V}{\lambda} \frac{\epsilon_2(\lambda)}{[\epsilon_1(\lambda)+2\epsilon_m]2+\epsilon_2(\lambda)^2} \tag{3.2}$$

$$\sigma_{sca} = \frac{32\pi^4\epsilon_m^2\,\sigma_{ext}=\frac{18\pi\epsilon_m^{\frac{3}{2}}V}{\lambda}}{\lambda^4}\ \left(\frac{(\epsilon_1-\epsilon_2)+\epsilon_2{}^2}{\epsilon_1+2\epsilon_2)+(\epsilon_2{}^{2)}}\right)^2 \tag{3.3}$$

Let V denote the volume of the particle.

During the mid-1800s, Michael Faraday carried out the initial methodical examination of the distinctive optical properties of gold colloid solution. He described the solution as "an aesthetically pleasing ruby-colored liquid" and noted that even a slight change in particle size resulted in a range of different colors. Mie[41] was inspired by Faraday's theories to create the aforementioned theoretical work.

3.3 Effect of Nano particle Shape, Size and Material

3.3.1 Nano Size Particle and Aspect Ratio

The size, shpe, and compositon of metal nanopartiles have a considerable impact on their LSPR capabilities. According to Mie's hypothesis, the absorption of light is directly related to the radius (R) of spherical particles that are very much lower than the λ (2πR, λ). Likewise, the scattering

magnitude of cross-section is precisely relate to the radius (R). When dealing with very small particles, absorption is the main element that determines the extinction of LSPR (Localized Surface Plasmon Resonance), while scattering becomes increasingly significant as the particle size grows [17]. The transition point for gold nanospheres takes place at around 80 nm in terms of partile diameter. Furthermore, phenomena is also observed, in addition to the well-established link between particle size and plasmon resonance wavelength. In 1909, Richard Zsigmondy, contemporaneous with Gustav Mie [41], observed the phenomena of gold colloid particles using dark field microscopy during his initial tests. The width of the plasmon resonence is contingent upon the dimensions of the particles. The broadening of the line is attributed to a combination of interband transitions, which result in a wider line for smaller partiles, and greater order plasmon modes, which lead t alarger line for larger particles.

3.3.2 Nano particle Shape

The sensitivity is generally largely dependents on the particals geometry. Specifically, particles with sharp ends have significantly higher refractive index sensitivity than those expected solely from their aspect ratios [15]. Many novel nanoparticle forms with mostely-increasing RI sensitivities has been produced over the last ten years. In the study of Mock et al., the spectrum of Au nanoparticles is varying forms (cubes, triangles, and spheres) but the volumes were connected with the structures, providing a striking example of the impact of particle shape on LSPR features. Furthermore, the sensitivity of the particles' RI was examined at the single-particl level, and it founded that the sensitivity of Ag nanotriangles (350 nm/RIU) was significantly higher than that of spheres (160 nm/RIU) [40]. Another illustration of this was provided by Sun et al., who showed how gold nanosphres and nanoshalls with the same diameter differed in their sensitivity to refractive index. They represent that the sensitivity of the nanoshells (409 nm/RIU) was significantly higher than that of the spheres (60 nm/RIU) [5]. Particularly high refractive index sensitivity is seen in particles with sharp ends, such as nanotriangles and bipyramid

It is crucial to ascertain whether the varying sensitivity of RI are due to inherent properties of particle form or the fluctuating PR wavelengths of the particles (as influenced by the optical features of the metal at that specific wavelength). The sensitivity of a plasmon resonance to refractive index increases as the resonance becomes more red-shifted (lower in energy) for a specific composition of materias. Miller and Lazarides' theoretical research illustrates that the responsiveness of nanoparticles to changes in RI, especially those with elevated sensitivities, exhibits a linear relationship with the wavelength of plasmon resonance.

3.3.3 Nano particle Material

Generally for LSPR sensing research has utilized silver or gold nanoparticles. Au is oftn chosen for its chemical stability and oxidation resistance [30]. However, Ag has a more sensitive refractive index and greater resonances. This is illustrated by contrasting gold and silver nanoparticles that have comparable sizes and shapes. Particles having sharp ends, such as nanotriangles and bipyramids, has a particularly higher sensitivity to changes in RI. The RI sensitivity for spheres with a diameter of 50-60 nm is 60 nm/RIU[30]. for gold47's plasmon resonance at 530 nm, and 160 nm/RIU for silver's plasmon resonance at 435 nm. For nanocubes ranging in size from 30 to 50 nm,[31] the sensitivity of refractive index is 83 nm/RIU for gold43 and 146 nm/RIU for silver at a plasmon resonance of 510 nm. This serves as an extra example. Influence of material composition [33] The table displays the LSPR (Localized Surface Plasmon Resonance) of particles that have comparable shape and size

Table 1 : Effect of material composition LSPR of particles of similar shape and size [15]

Particle Type	**Size (nm)**	**LSPR Peak (nm) (nm/IRU)**	**Senstivity**
Au nanosphere	50	530	60
Ag nanosphere	60	435	160
Au nanoCube	44	538	83
Ag nanoCube	30	510	146

Table : 2 tuneable LSPR range for different structures [42]

Ref No.	Description of Nanostructure	Tuneable LSPR range
Huang et al. [2019]	Core shell Spiky nanoparticles	150nm (650nm to 800nm
Wang et al. [2019]	Waveguide with 2 rectangular cavity	176 nm (585nm to 761)
Liu et al. [2022]	Nano sphere/Nano shell/Nano star/ Nano flower	142 nm (551nm to 693nm)
Yamada et al. [2022]	Nano holes with Edge structure	279nm (785nm to 1064nm)

3.4 Beyond Nano Particles

LSPR sensors that utilize a complex extended structure inspit of a simple nanoparticle plasmon resonance which belongs to a different category. Plasmonic extinction spectra with robust, concentrated resonances and heightened sensitivities to refractive index can be achieved by leveraging nanoparticle's geomatery arrays and other planar nanostructures. Henzie et al. [15] have utilized innovative lithography techniques to produce gold films with multiscale nanohole arrays that exhibit several plasmon resonances in the near-IR region of the transmission spectrum. Nanostructures have garnered significant interest for their capacity to detect Fano resonances in their extinction spectra through the use of LSPR [15]. Fano resonances manifest in asymmetrical nanostructures, such as nonconcentric coreshell particles, when a non-light-coupling plasmon mode, known as a "dark" mode, interferes with the typical light-coupling plasmon mode, referred to as a "bright" mode. In theory, the steep drop in extinction is supposed to be greater sensitive to changes in RI. Improvee RI sensing can be achieved through both the optimization of metallic nanostructure design and through meticulous substrate design, the plasmonic structure is securely held in position. Dmitriev et al. demonstrated that by increasing the metal nanoparticles above the substrate using a dielectric pillar, the sensitivity of the refractive index can be significantly enhanced. This results in an increased amount of available space.

Methods to access the area with heightened e-field intensity. This increased the sensitivity of nanodiscs by a factor of two [15]. While optimizing the size, shape, and composition of nanoparticles is undeniably advantageous, it alone does not provide a comprehensive solution to the challenge of broadening the application of LSPR in the fields of science and technology. Important factors to consider are the stability and availability of the sensor substrates, their

chemical interaction with the analyte, and the need for accurate and quantitative real-time measurements.

3.5 Sensors Based on LSPR

3.5.1 Biological Sensors Based on LSPR -

Generally characteristics of LSPR sensing indicate the potential application of this technology in biological and biomedical testing. Sensory LSPR does not require the use of labels. Most tests, such as ELISAs, employ precise exposure and rinsing techniques that utilize a molecular approach to generate the which is signal prior to detecting the antigen target. During an endpoint test, the antigen target is not immediately detected. Instead, it forms a bond with a separte antibody and generates a signal. Label-free assays detect a feature of the target antigen molecule striaghtly . By using technology, it becomes feasible to examine the rate at which molecules bond to each other in a live setting and to constantly monitor the amount of the desired substance present on the sensor. Label-free assays are more easier than end-point assays because their requirements one capture antibody and allow direct detection with less complex procedures[17]. utilization of LSPR nanoparticle in label-free investigations reduces diffusion-limited mass transfer and localized the sensational area, hence decreasing amount of analyte required to generate a signal. Label-free assays have low sensitivity because they lack amplification.

Biotin – Streptavidin

The biotin-streptavidin interaction is commonly studied in the development of biological assays due to its strong and specific binding properties. Biotin-streptavidin reagents are readily available for use in bio conjugation techniques. Biotin is very suitable for LSPR sensing because it can adhere to the surface of nanoparticles and accurately detect the index refraction of the larger streptavidin protein. There is multiple data on the interaction between biotin and streptavidin using LSPR assays. The reported streptavidin sensitivity spans a concentration range from picomolar to micromolar [17-19]. While the affinity may be influenced by experimental settings, it should not exhibit such a significant variation in orders of magnitude, which is somewhat surprising considering the diverse range of performance. The observed volatility mostly stems from changes in the Keq values of the dose-response curves.

Antibody- Antigen

Usually, a surface-active molecule (SAM) and traditional bioconjugate linkers are employed to attach capture antibodies to the surface of the nanoparticle. Most articles utilize the dose-response curve to establish the sensitivity. The sensitivity is determined by the SNR ratio and binding constant, as previously stated. In addition to the results obtained from the biotin-streptavidin interaction, several immunoassay studies yield equilibrium constant (Keq) values in the range of 109 – 1010 M-1 [19]. In addition to the interactions between biotin and streptavidin and antibodies and antigens, the sensing of LSPR has also been employed to study nucleic acid hybridization and several other interactions such as protein-carbohydrate, cytochrome inhibitor, aptamer-protein, and toxin-receptor interactions [18]. In addition, LSPR bioassays have been conducted in complex fluids such as whole blood and serum.

3.5.2 LSPR - Based Chemical Sensors

Gas Sensor

Lately, there has been significant enthusiasm in developing LSPR sensors for both chemical and biological sensing purposes because to its advantageous characteristics of being label-free and rapid.. Cheng et al. have successfully explain the detection of gaseous volatile organic compounds (VOCs), such as toluene, using LSPR sensing [28]. During their initial investigation, the researchers utilized the peak wavelength and the integrated total magnitude of the particles' extinction to monitor the adsorption of these compounds onto silver and gold nanoparticles that are bound to a substrate, as well as gold nanoshells. The answer was prompt and capable of being reversed[29] . The detection limit for toluene in this refractive index sensing approach was 5 parts per million (ppm).

pH Sensors

Plasmonic nanoparticles have also been utilized in various pH sensing techniques, sometimes in combination with pH-sensitive polymers. Nuopponen et al. developed a pH sensor by utilizing Au nanospheres which is covered with the pH-responsive block copolymer PMAA-b-PNIPAM, where PMAA stands for poly(methacrylic acid) and PNIPAM refers for poly(N-isopropylacrylamide). The particles coated with polymer were dispersed in a water-based solution, and within the pH range of 5 to 8, they underwent acid-base accumulation. Particle agglomeration is a permanent phenomenon that cannot be reversed, and it is also influenced by temperature. Mack

et al. later revealed a plasmonic crystal-based pH sensor [25]. The plamonic crystal consisted of a polymer layer with a patterned arrangement of nanowells measuring 480 nm, which were coated with a layer of gold. Subsequently, a hydrogel was applied to the substrate. The hydrogel was composed of 2.0 weight % acrylic acid (AA), 1.1 weight % ethylene glycol dimethacrylate (EGDMA) cross-linker, 3.7 weight % photoinitiator (PI), 55.5 weight % hydroxyethyl methacrylate (HEMA), and aqueous Brij 58 surfactant. With an increase in pH, the hydrogel underwent inflation, resulting in a decrease in its density, refractive index, and a blue shift in the transmission spectrum's several LSPR peaks [43].

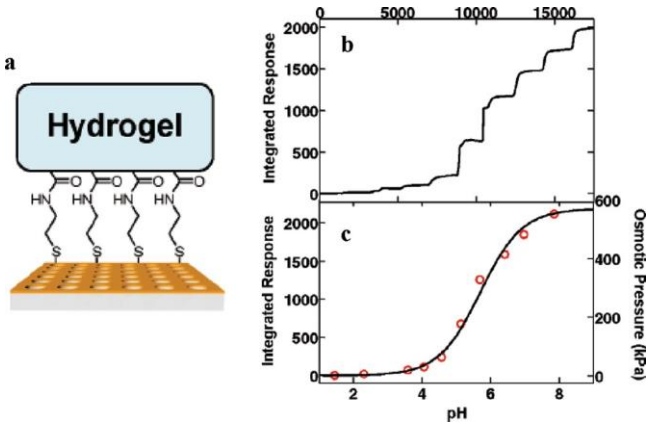

Figure 3.2 (a) The Hydrogen- modified plsmonic crystal pH sensor of Mack [25] et al. (b) Integrated transmitted intensity response to pH. (c) Calculated osmotic pressure experienced by the hydrogel at each pH Value [25]

3.5.2 Technological Advances in LSPR Sensing

Multiplexing

In order for LSPR sensors to be able to compite with ELISA and other conventional assays as large -throughput laboratory and clinical screening tools, this technique should be comparable to effectively handle higher amounts of samples. Endo et al [26].conducted an experiment where they arranged 300 small areas containing tiny amounts solutions of antibody on a thin layer of Au-coated nanospheres[44]. This experiment showcased the promising capabilities of this technology. Subsequently, a scanning optical probe was employed to quantify the optical absorbance of the film, enabling a comparison of the binding strength of each antibody to the analyte. Instead of quantifying the shift in the LSPR peak, the alteration in integrated absorbance was quantified[45]. Antigens detected at100 picograms per milliliter of solution concentrations as low as [46].

Integration with Microfluidics

In order to be compatible with clinical samples, LSPR sensors must possess the capability to detect targets within highly minute sample quantities. Additionally, it is advantageous to possess a high level of throughput and speed. Microfluidics is the predominant technique employed to address this problem, and there have been promising initial efforts to integrate microfluidic devices with LSPR sensing. Hiep et al. have built an chip based on LSPR that features a solitary microfluidic channel and can hold up to 1 μL of sample. The LSPR substrate consists of a flat gold sheet with a gold-capped nanosphere layer on top [27]. This method was used for bulk refractive index sensing of glucose solutions and real-time kinetics specific immunodetection of insulin with a detection limit of 100 ng/mL. Huang et al. have recently demonstrated a similar LSPR-microfluidic chip composed of gold nanosphere sheets. This method utilized a sample volume of 2.5 μL and incorporated two microfluidic channels running in parallel, along with an automated sampling equipment. The sensor demonstrated a precision of 10^4 RIU in measuring RI. Immunosensing was also demonstrated using this setup by the measurement of biotin/antibiotin binding. Both of these microfluidic chips successfully detected the LSPR signal using conventional UV-vis absorbance spectrometers.

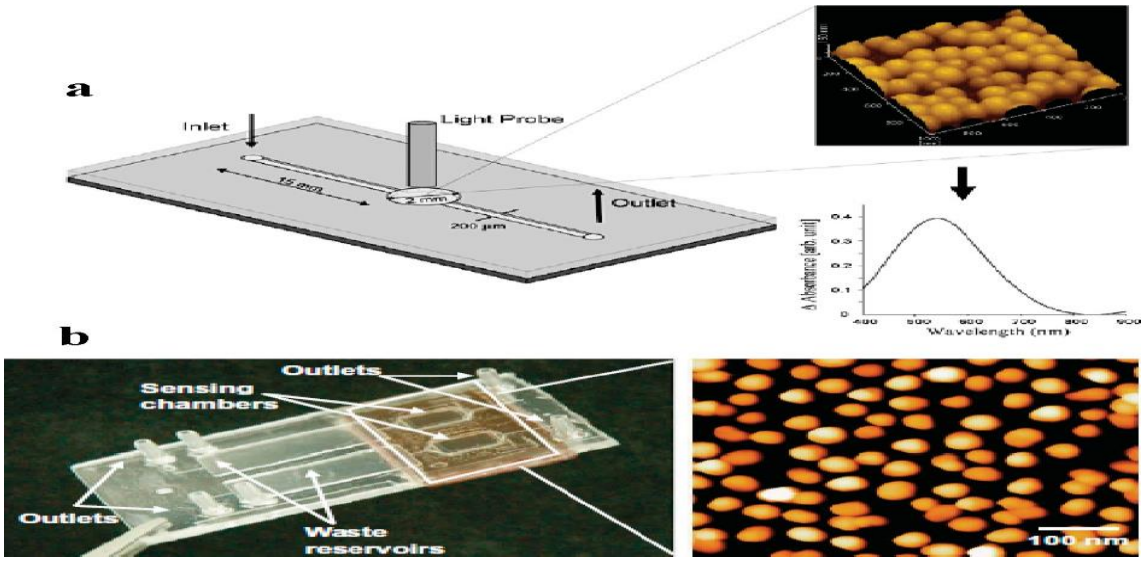

Figure 3.3. The Integrated microfluidic Chips (a) nanospheres with a gold cap covering a flat gold film (b) LSPR-microfluidic chip utilizing gold nanosphere films

Optical Fiber Probe

Plasmonic nanoparticles and optical fibers can collaborate to enable (LSPR) detection with higher sensitivity, even at minuscule amounts, over long distances, and even within biological organisms.

Cheng et al [28]. developed a LSPR sensor -based on fiber by attaching Au nanospheres to the end of the fiber. The fiber's reflectance spectra indicated LSPR of the particles. By employing this method, they explain the ability to detect nickel ions, calculating the RI of a large sample, and observe the binding of biotin and streptavidin [29] Mitsui et al. developed a LSPR sensor based on fiber- that eliminated needs for a spectrometer and white light source by solely utilizing the total reflection intensity of a red light-emitting diode. One of the main challenges in molecular detection utilizing LSPR is to improve the signal-to-noise ratio of LSPR peak wavelength shift measurements in order to enhance the molecular detection capabilities of these single particle systems.

Figure 3.4 Different types of optical sensors

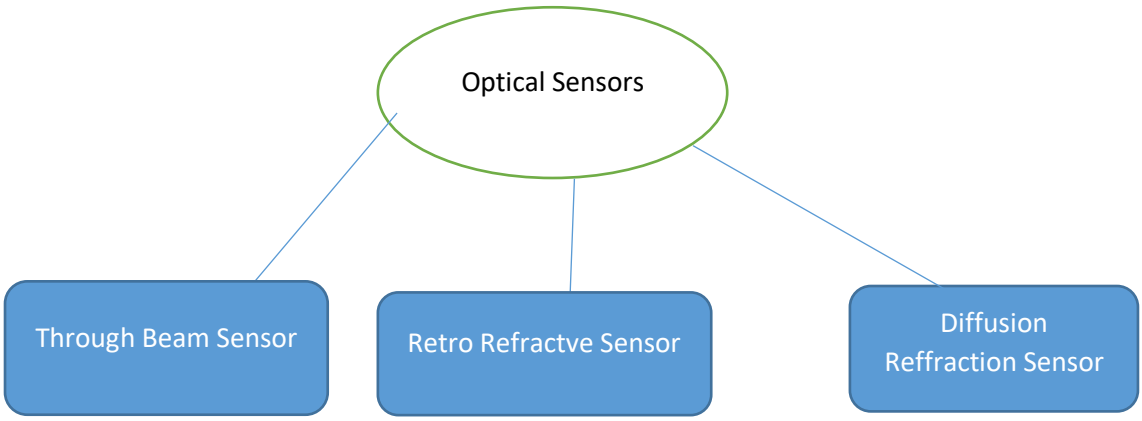

CHAPTER 4

SIMULATION

4.1 Introduction of software

FDTD: The Finite-Difference Time Domain method The time-domain approach is a highly efficient and precise method for simulating optical devices at the nanoscale. While primarily a method for analyzing time-domain data, frequency analysis can also be conducted using the Discrete Fourier Transform (DFT) and Fast Fourier Transform (FFT) [47]. It solves Maxwell's equations without making any physical approximations. Some typical applications of this technology include LEDs, solar cells, filters, optical switches, semiconductor-based photonic devices, sensors, nano- and micro-lithography, nonlinear devices, and meta-materials with a negative index of refraction[47].

FDTD Method Overview:

Finite-Difference Time-Domain (FDTD) method

Rigorous and powerful modelling tool

Nano-scale optical devices

Time-Domain Solution:

Time-domain analysis

Solves Maxwell’s equations directly

No physical approximation

Frequency Analysis:

Fast Fourier Transform (FFT)

Discrete Fourier Transform (DFT)

Frequency analysis capabilities

Applications:

Light Emitting Diodes (LEDs

Solar cells

Optical filters

Optical switches

Semiconductor-based photonic devices

Sensors

Nano- and micro-lithography

Nonlinear devices

Meta-materials (negative index of refraction)

Nano-Scale Optical Devices:

Modelling at the Nano-scale

Precision in optical device simulation

High accuracy in results

Diverse Applications:

Broad range of applications

Versatile tool for various devices

Enables comprehensive optical device design

Maxwell's Equations:

Direct solution of Maxwell's equations

Fundamental basis for electromagnetic field analysis

Meta-Materials:

Modelling negative index of refraction

Meta-material characterization

Unique optical properties

Technological Impact:

Advancing LED technology

Enhancing solar cell efficiency

Improving semiconductor-based photonic devices

Enabling innovative sensor designs

Simulation Capabilities:

Accurate simulation of optical phenomena

Realistic representation of device behaviour

Facilitates optimization and design iterations

The Finite-Difference Time-Domain (FDTD) method is employed by the Full WAVE simulation tool to conduct a comprehensive simulation of photonic structures, taking into account both magnitude and direction of electromagnetic fields. This instrument is highly sophisticated and is used to study the way light travels in various photonic structures. It may be applied to circuits, nano photonic devices, integrated and fiber-optic waveguide devices, as well as photonic crystals.

4.2 Benefits

The advanced utilization of a well-developed FDTD algorithm enables a broad spectrum of simulation and analysis functionalities. Advanced features enable the creation of a clustered simulation environment, resulting in significant improvements in computational performance and efficiency.

Plasmonics nanostructures can be designed using several geometries, including nanospheres, nanorods, nanodiscs, nanocubes, nanocylinders, and others. These nanostructures can be utilized

for a wide range of plasmonics applications, including chemical and bioanalyte sensors, SERS, and nanophotonic devices such as communication switches and modulators, among others.

By using FDTD simulator we do simulations for nano structures like Disc, Circle and Sphere for getting E- field Enhancement Vs Wavelength (nm). As we know that Shape, size and material effects E- field enhancement. So we use different materials, size and shape of nano structures.

Nano Structures

Disc

Structure 1 (A): - In this structure

Number of Disc = 2.

Material = Silver

Radius =40nm

Height =50nm

PML thickness (8 layer)

Mesh accuracy (2)

Source distance (1000nm)

Source Type = Plane Wave Source

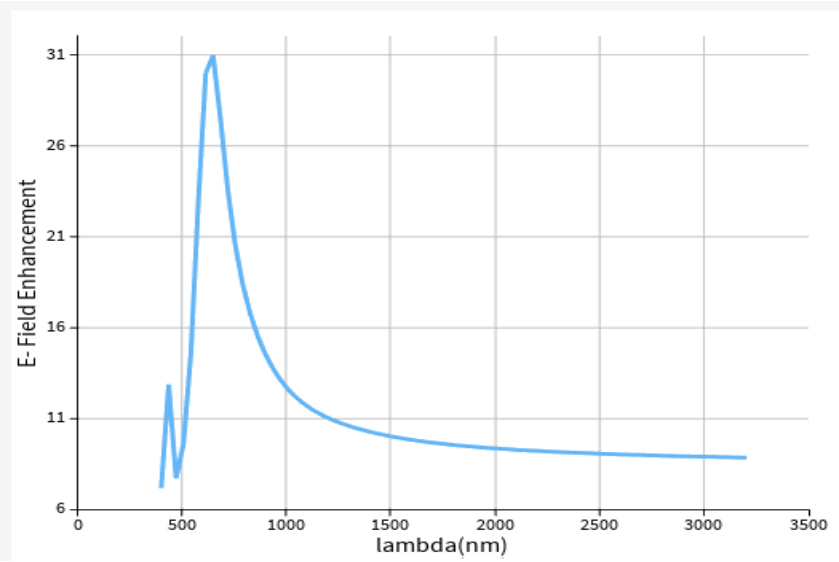

Figure: 4.2(a) Graph between Electric Field Enhancement Vs Wavelength (nm)

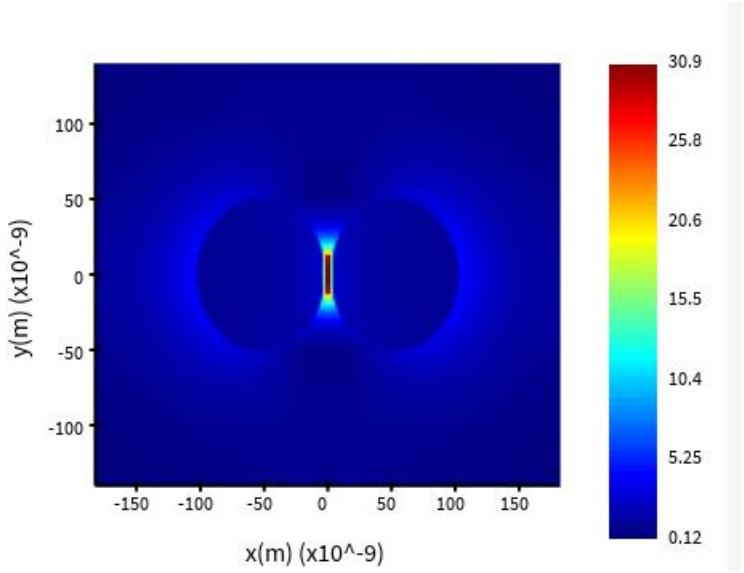

Figure 4.2(b) Image for Electric Field Enhancement

Structure 1 (B): - In this structure

Number of Disc = 2.

Material = Silver

Radius =80nm

Height =50nm

PML thickness (8 layer)

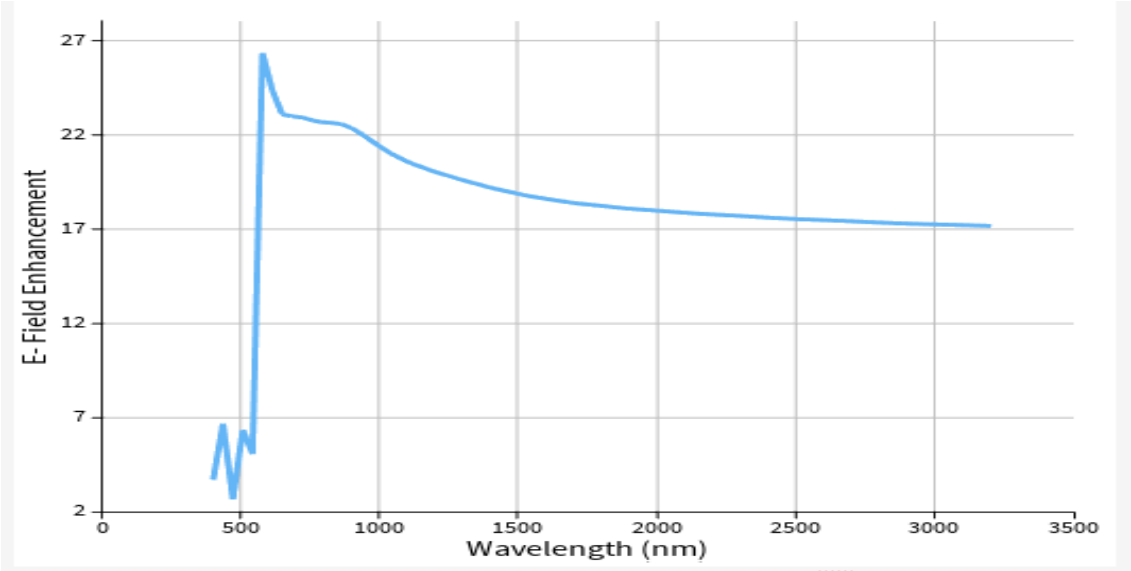

Figure 4.2(c) Graph between Electric Field Enhancement Vs Wavelength (nm)

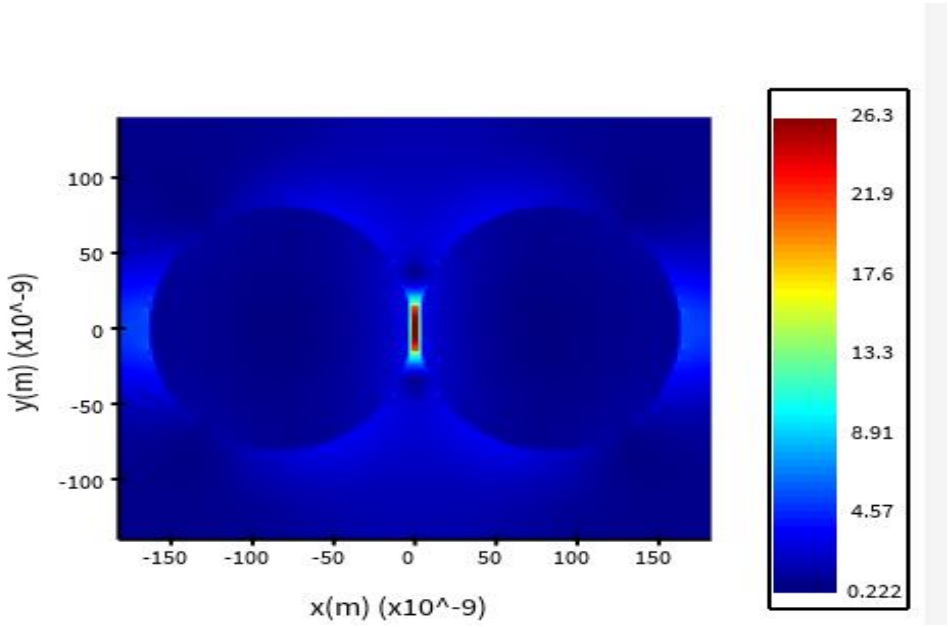

Figure 4.2(d) Image for Electric Field Enhancement

Structure 1 (C): - In this structure

Number of Disc = 2.

Material = Silver

Radius =20nm

Height =50nm

PML thickness (8 layer)

Mesh accuracy (2)

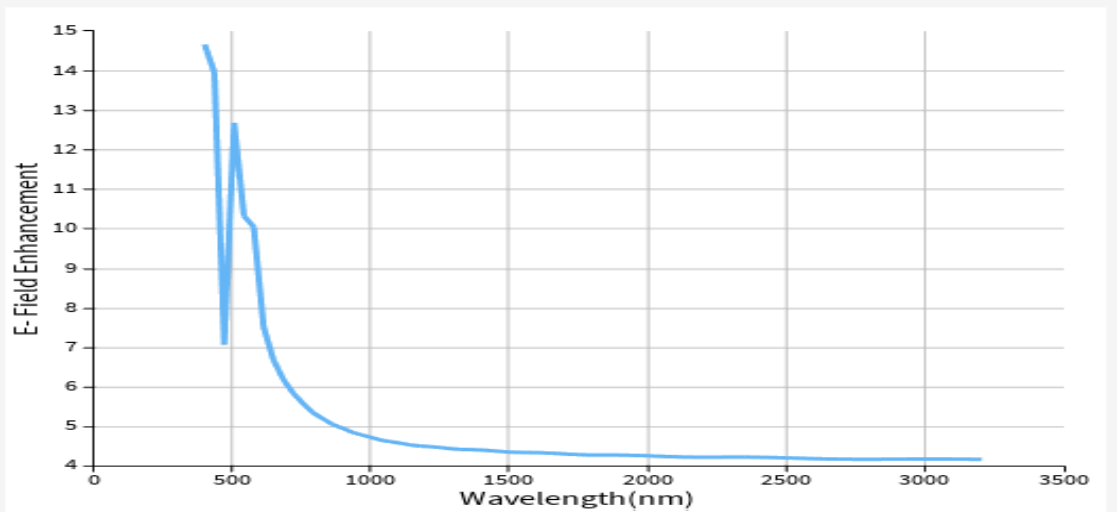

Figure: 4.2(e) Graph between Electric Field Enhancement Vs Wavelength (nm

Based on the above structure, it is evident that the E-Field Enhancement decreases when the radius of the structure is increased or decreased at a specific wavelength. Therefore, assuming a radius of 40nm is a precise estimation for calculating the E-Field Enhancement at that particular wavelength. and the wavelength range is small as compare to other nanostructures it can be use for Color Sensors. So, next we will proceed to discuss the Ring nanostructure.

Ring

Structure 2 (a) : This structure Gap between 2 Rings= 5nm

Number of Rings = 2.

Material = Silver (Ag Soft)

Outer Radius= 40nm, Inner = 35

PML thickness (8 layer)

Mesh accuracy (2)

Source distance = 1000 nm (Plane Wave Source)

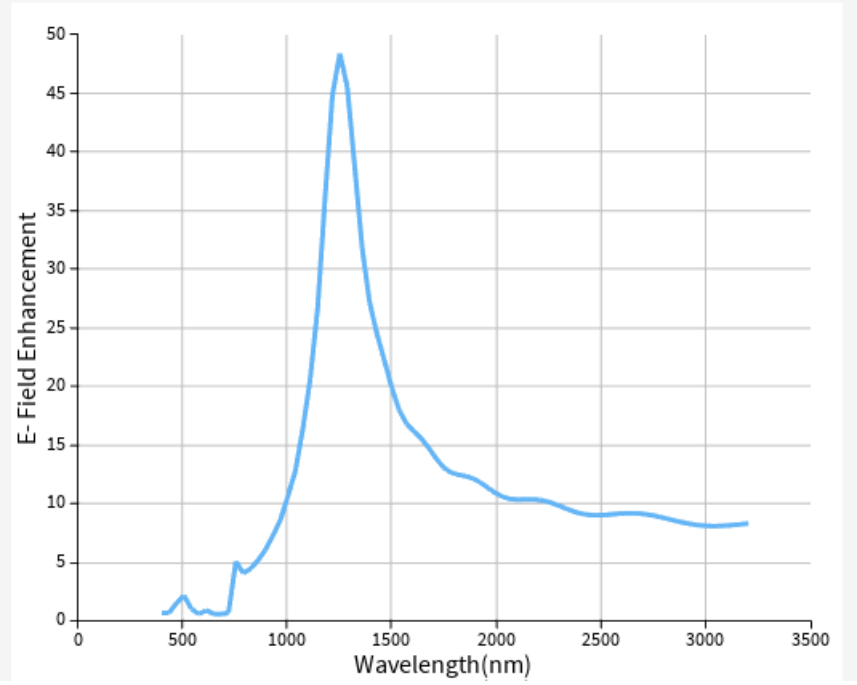

Figure: 4.2(f) Graph between Electric Field Enhancement Vs Wavelength (nm)

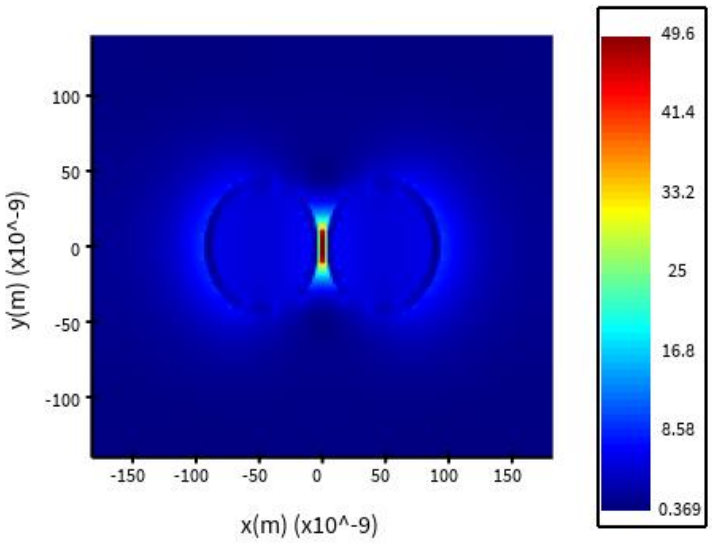

Figure 4.2(g) Image for Electric Field Enhancement

Structure 2 (b): This structure Gap between 2 Rings= 5nm

Number of Rings = 2.

Material = Silver (Ag Soft)

Outer Radius= 65 nm, Inner = 60

PML thickness (8 layer)

Mesh accuracy (2)

Source distance = 1000 nm (Plane Wave Source)

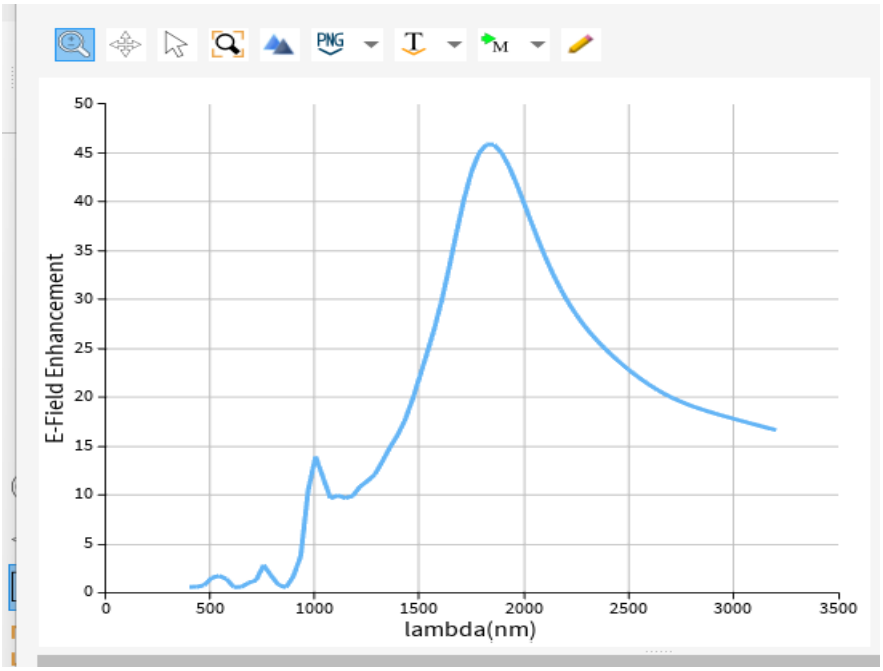

Figure: 4.2(h) Graph between Electric Field Enhancement Vs Wavelength (nm)

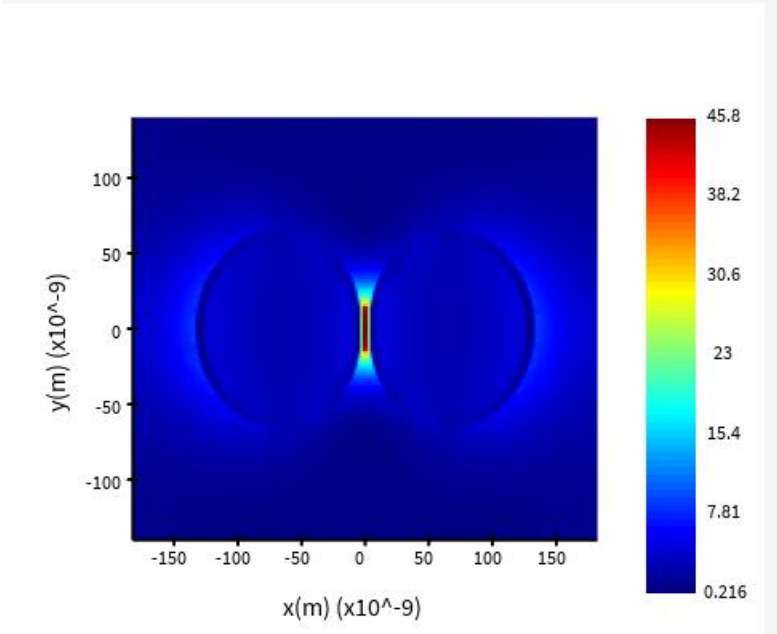

Figure 4.2(i) Image for Electric Field Enhancement

Structure 2 (c): This structure Gap between 2 Rings = 10 nm

Number of Rings = 2.

Height =50 nm

Material = Silver (Ag Soft)

Outer Radius= 65 nm, Inner = 60

PML thickness (8 layer)

Mesh Accuracy 2

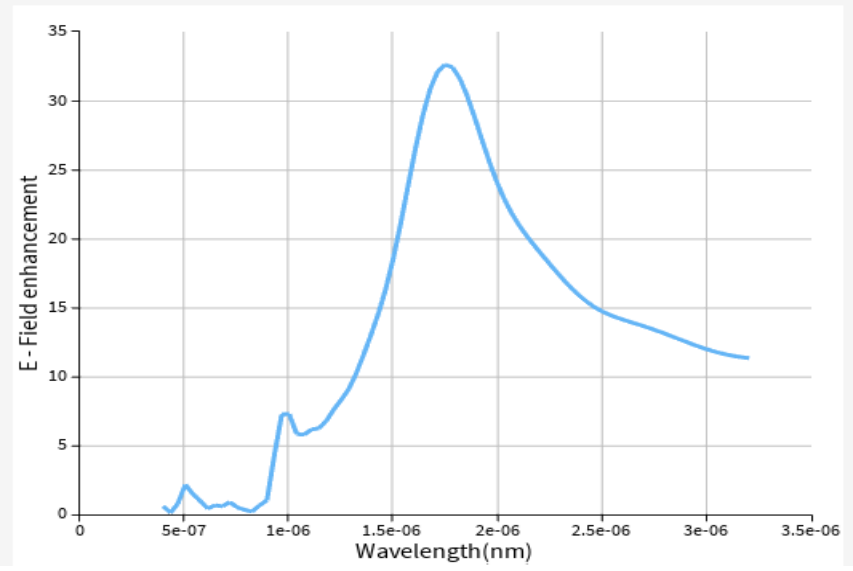

Figure: 4.2(j) Graph between Electric Field Enhancement Vs Wavelength (nm)

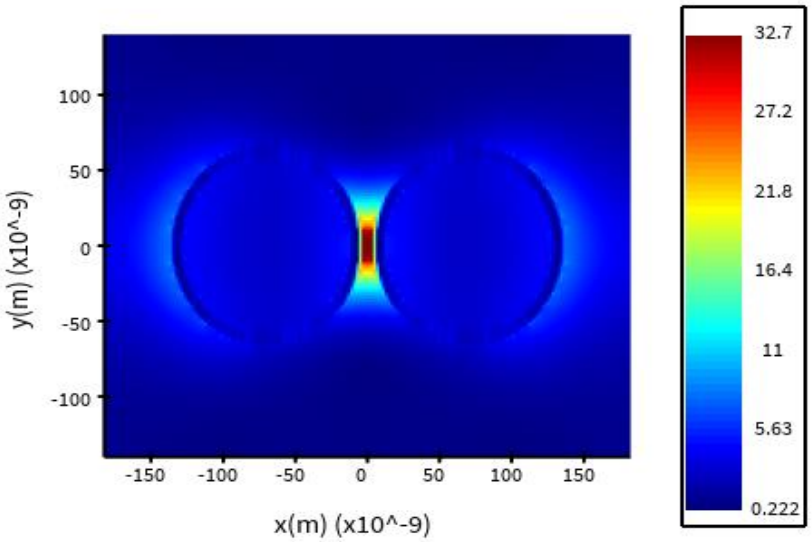

Figure 4.2(k) Image for Electric Field Enhancement

Structure 2 (d): This structure Gap between 2 Rings =10 nm

Number of Rings = 2.

Material = Gold (Au Soft)

Outer Radius= 40 nm, Inner = 35

Height =50 nm

PML thickness (8 layer)

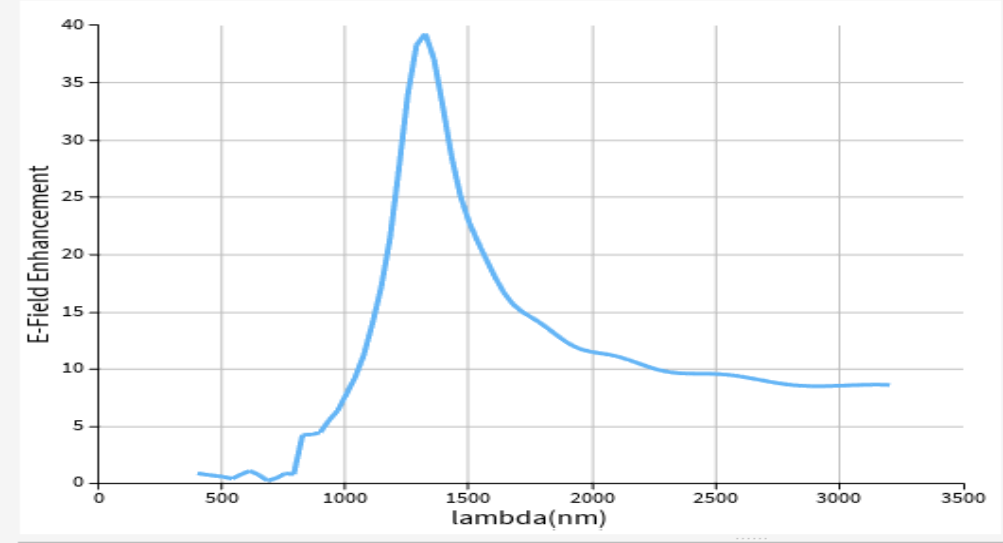

Figure: 4.2(l) Graph between Electric Field Enhancement Vs Wavelength (nm)

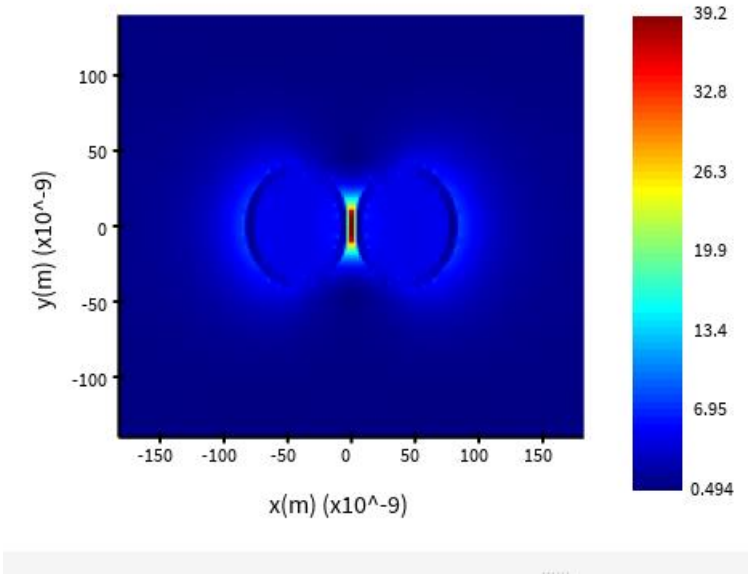

Figure 4.2(m) Image for Electric Field Enhancement

Structure 2 (e): This structure Gap between 2 Rings =5nm

Number of Rings = 2.

Material = Gold (Au Soft)

Outer Radius= 40 nm, Inner = 35

Height =100 nm

PML thickness (8 layer)

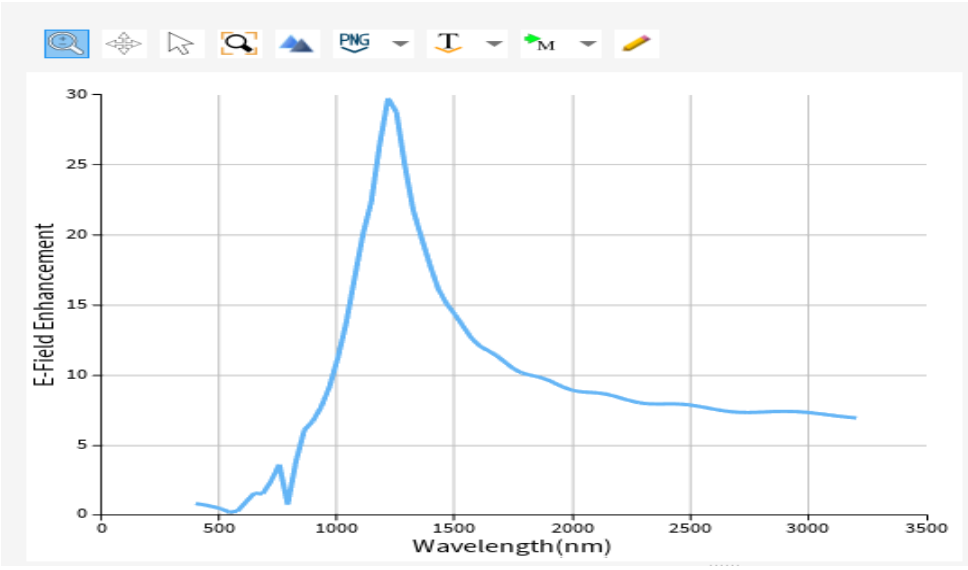

Figure: 4.2(n) Graph between Electric Field Enhancement Vs Wavelength (nm)

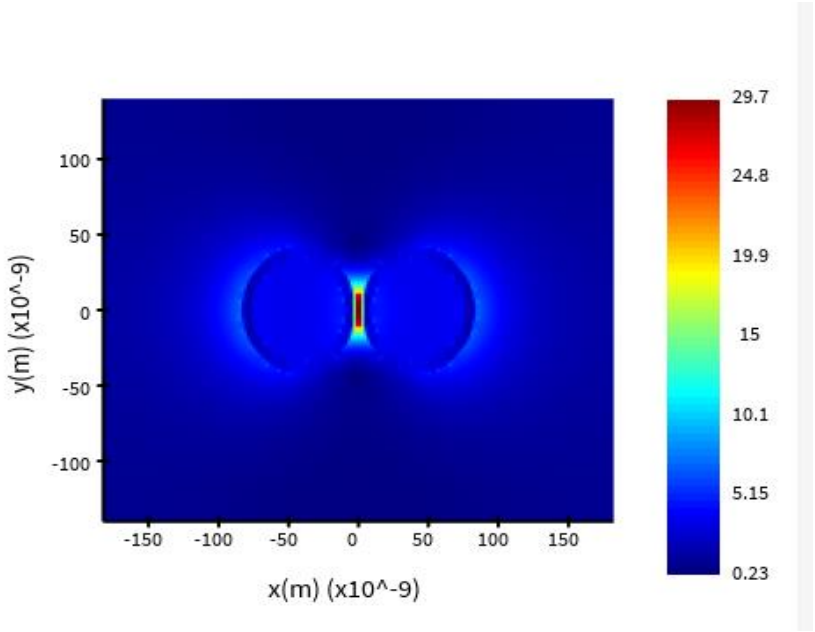

Figure 4.2(o) Image for Electric Field Enhancement

As the radius of both rings is increased, the magnitude of the E-field enhancement decreases, while the range of wavelengths increases. By widening the distance between both rings from 5nm to 10nm, the spectrum of wavelengths has expanded. From the identical structures of the gold and silver material nanostructures, it is evident that when the gap, source distance, height, and radius are all the same, the gold material structure exhibits a higher value for E-Field Enhancement compared to the silver material structure. This discrepancy is attributed to the gold material's greater absorption of light. The range observed in this structure falls under the infrared (IR) category. This structure is suited for application in Biomedical Sensors.

Structure: 3 (a)

Sphere

This structure Gap between 2 Spheres =5nm

Number of Spheres = 2.

Material = Silver (AgSoft)

Outer Radius= 40 nm

PML thickness (8 layer)

Source distance = 1000nm

Source Type = Plane wave

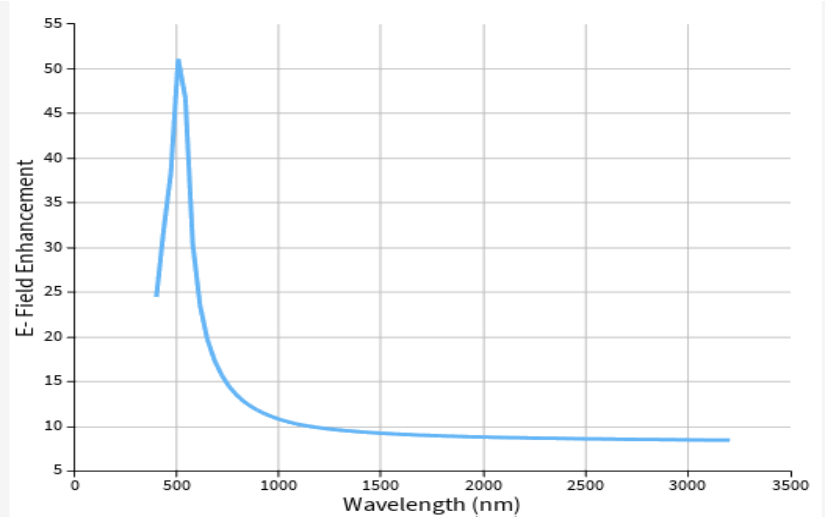

Figure: 4.2(p) Graph between Electric Field Enhancement Vs Wavelength (nm)

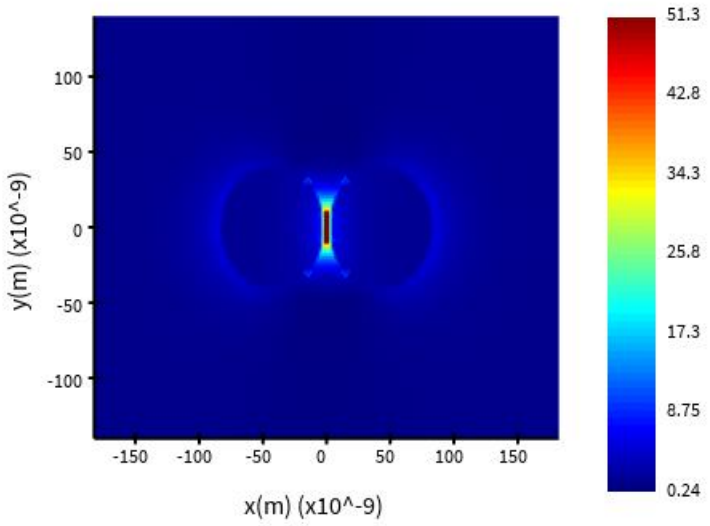

Figure 4.2(q) Image for Electric Field Enhancement

CHAPTER 5

CONCLUSION AND FUTURE SCOPE

We have simulate the different nanostructures with effect of LSPR. In the thesis we find that optical sensors wavelength range is from 400nm to IR So from above structures we can use any structure as per our requirements for the optical sensor. In spite of that Form the above simulation of different structures we have seen that the structure which gives more E-Field Enhancement over high value of wavelength is Ring nano structure. Moreover we saw that as the radius of both rings is increased, the magnitude of the E-field enhancement decreases, while the range of wavelengths increases. By widening the distance between both rings from 5nm to 10nm, the spectrum of wavelengths has expanded. From the identical structures of the gold and silver material nanostructures, it is evident that when the gap, source distance, height, and radius are all the same, the gold material structure exhibits a higher value for E-Field Enhancement compared to the silver material structure. This discrepancy is attributed to the gold material's greater absorption of light. The range observed in this structure falls under the infrared (IR) category. This structure is suited for application in Biomedical Sensors. Sphere and Disc nano structures can be used for color sensors because its wavelength range exist for that type of sensors.

Optical sensors possess the capacity to perceive light, usually within a certain range of the electromagnetic spectrum, including ultraviolet, visible, and infrared wavelengths. The sensor detects the wavelength, frequency, or polarization of light and turns it into an electric signal by the photoelectric effect. The measurable quantities that can be detected by various optical sensors include temperature, velocity, liquid level, pressure, displacement (position), vibrations, chemical species, force radiation, pH value, strain, acoustic field, and electric field.

REFERENCES

[1] Bohren, C. F.; Huffman, D. R. Absorption and Scattering of Light by Small Particles, 2nd ed.; Wiley-Interscience: New York, 1998.

[2] Anderson, L. J. E.; Mayer, K. M.; Fraleigh, R. D.; Yang, Y.; Lee, S.; Hafner, J. H. J. Phys. Chem. C 2010, 114, 11127.

[3] Mock, J. J.; Barbic, M.; Smith, D. R.; Schultz, D. A.; Schultz, S. J. Chem. Phys. 2002, 116, 6755

[4] Sherry, L. J.; Chang, S.-H.; Schatz, G. C.; van Duyne, R. P.Nano Lett. 2005, 5, 2034.

[5] Link, S.; El-Sayed, M. A. J. Phys. Chem. B 1999, 103, 4212.

[6] Miller, M. M.; Lazarides, A. A. J. Phys. Chem. B 2005, 109, 21556.

[7] Mock, J. J.; Smith, D. R.; Schultz, S. Nano Lett. 2003, 3, 485.

[8] Sun, Y.; Xia, Y. Anal. Chem. 2002, 74, 5297.

[9] Chen, H. J.; Kou, X. S.; Yang, Z.; Ni, W. H.; Wang, J. F. Langmuir 2008, 24, 5233.

[10] Nehl, C. L.; Liao, H. W.; Hafner, J. H. Nano Lett. 2006, 6, 683

[11] Sherry, L. J.; Jin, R.; Mirkin, C. A.; Schatz, G. C.; Van Duyne, R. P. Nano Lett. 2006, 6, 2060.

[12] Liu, M.; Guyot-Sionnest, P. J. Phys. Chem. B 2005, 109, 22192

[13] Bukasov, R.; Shumaker-Parry, J. S. Nano Lett. 2007, 7, 1113.

[14] Sun, Y.; Xia, Y. Anal. Chem. 2002, 74, 5297.

[15] Henzie, J.; Lee, M. H.; Odom, T. W. Nat. Nanotechnol. 2007, 2, 549.

[16] Liu, N.; Weiss, T.; Mesch, M.; Langguth, L.; Eigenthaler, U.; Hirscher, M.; Sonnichsen, C.; Giessen, H. Nano Lett. 2010, 10, 1103.

[17] Marinakos, S. M.; Chen, S. H.; Chilkoti, A. Anal. Chem. 2007, 79, 5278

[18] Nath, N.; Chilkoti, A. Anal. Chem. 2002, 74, 504.

[19] Haes, A. J.; Van Duyne, R. P. J. Am. Chem. Soc. 2002, 124, 10596

[20] Holmberg, A.; Blomstergren, A.; Nord, O.; Lukacs, M.; Lundeberg, J.; Uhlen, M. Electrophoresis 2005, 26, 501.

[18] Mayer, K. M.; Lee, S.; Liao, H.; Rostro, B. C.; Fuentes, A.; Scully, P. T.; Nehl, C. L.; Hafner, J. H. ACS Nano 2008, 2, 687.

[19] Lee, S.; Mayer, K. M.; Hafner, J. H. Anal. Chem. 2009, 81, 4450.

[20] Mayer, K. M.; Lee, S.; Liao, H.; Rostro, B. C.; Fuentes, A.; Scully, P. T.; Nehl, C. L.; Hafner, J. H. ACS Nano 2008, 2, 687.

[21] Haes, A. J.; Chang, L.; Klein, W. L.; Van Duyne, R. P. J. Am. Chem. Soc. 2005, 127, 2264.

[22] Englebienne, P. Analyst 1998, 123, 1599.

[23] Chen, K. J.; Lu, C. J. Talanta 2010, 81, 1670.

[24] Karakouz, T.; Vaskevich, A.; Rubinstein, I. J. Phys. Chem. B 2008, 112, 14530.

[25] Mack, N. H.; Wackerly, J. W.; Malyarchuk, V.; Rogers, J. A.; Moore, J. S.; Nuzzo, R. G. Nano Lett. 2007, 7, 733.

[26] Endo, T.; Kerman, K.; Nagatani, N.; Hiepa, H. M.; Kim, D. K.; Yonezawa, Y.; Nakano, K.; Tamiya, E. Anal. Chem. 2006, 78, 6465.

[27] Hiep, H. M.; Nakayama, T.; Saito, M.; Yamamura, S.; Takamura, Y.; Tamiya, E. Jpn. J. Appl. Phys. 2008, 47, 1337.

[28] Cheng, S. F.; Chau, L. K. Anal. Chem. 2003, 75, 16.

[29] Tang, J. L.; Cheng, S. F.; Hsu, W. T.; Chiang, T. Y.; Chau, L. K. Sens. Actuators, B 2006, 119, 105.

[30]. Synopsys [Online] Available: https://www.synopsys.com/photonic-solutions/rsoft-photonic-device-tools/passive-device-fullwave.html

[31].file:///C:/Users/Lenovo/Desktop/Plasmonics_Circuit_and_system_level_evaluation_for_beyond_CMOS_applications.pdf

[32].https://www.researchgate.net/publication/320591772_Plasmonics_Circuit_and_system

- level_evaluation_for_beyond-CMOS_applications

[33]. https://en.wikipedia.org/wiki/Plasmonics

[34]. Synopsys [Online] Available: https://www.synopsys.com/photonic-solutions/product-applications/communications/modeling-ring-resonator.html

[35]. D. Hisamoto and T. Kaga, "A fully depleted lean-channel transistor -a novel verticalultra-thin SOI MOSFET," in Int. Electron Devices Meet., pp. 833–836, 1989

[36]. G. Moore, "Cramming More Components Onto Integrated Circuits," Proc. IEEE, vol. 86,pp. 82–85, jan 1998.

[37] .R. Kirchain and L. Kimerling, "A roadmap for nanophotonics," Nat. Photonics, vol. 1, pp. 303–305, jun 2007.

[38].Jonas Doeven speck[year2015–2016] Plasmonics_Circuit_and_system_level_evaluation_for_beyond_CMOS_applications.pdf by

[39]Moore'slaw.Available: https://www.google.com/search?q=moore%27s+law&sca_esv=588766249

[40] Faraday, M. Philos. Trans. R. Soc. London 1847, 147, 159.

[41] Mie, G. Ann. Phys. (Weinheim, Ger.) 1908, 25, 377.

[42] Dalal, K., & Sharma, Y. (2023). Tunable LSPR in Asymmetric Plasmonic Bowtie Nanostructures. Noida: IEEE

[43]Nuopponen, M.; Tenhu, H. Langmuir 2007, 23, 5352.

[44] Yu, C. X.; Irudayaraj, J. *Anal. Chem.* 2007, *79*, 572.

[45] Yu, C. X.; Nakshatri, H.; Irudayaraj, J. *Nano Lett.* 2007, *7*, 2300.

[46]Wang, C.; Irudayaraj, J. *Small* 2008, *4*, 2204.

[47] Ansys [online] Avilable: https://www.ansys.com/en-in.